U.PORTO

FEUP FACULDADE DE ENGENHARIA UNIVERSIDADE DO PORTO

INSTITUTO DE CIÊNCIAS BIOMÉDICAS ABEL SALAZAR UNIVERSIDADE DO PORTO

INSTITUTO DE INVESTIGAÇÃO E INOVAÇÃO EM SAÚDE UNIVERSIDADE DO PORTO

INEB Instituto de Engenharia Biomédica

Work in collaboration with:

FMUP FACULDADE DE MEDICINA UNIVERSIDADE DO PORTO

Dissertation
Integrated Master in Bioengineering

Pericardial fluid: from biochemical screening to therapeutic potential in ischemic heart disease

Daniel Pereira de Sousa

Supervisor: Diana Nascimento, PhD
Co-supervisor: Perpétua Pinto-do-Ó, PhD

September, 2018

ABSTRACT

Ischemic heart disease is the leading cause of death worldwide, being responsible for almost 9 million deaths annually. Among ischemic heart diseases, myocardial infarction is the major cause of morbidity and mortality. The pericardial fluid has been pointed as a potential source of molecular targets that can be modulated to promote regeneration or more efficient repair of the infarcted heart.

In pathological conditions the pericardial fluid becomes enriched in cytokines, growth factors and hormones likely secreted by cardiac cells, which by retrograde effect impact on vascular, epicardial cells and cardiomyocytes. Exosomes and microRNAs, in particular pro-fibrotic miRNA-21-5p, were also found in PF. As reservoir of active substances that affect the heart, PF has been recently considered a privileged source to investigate cardiac pathophysiologic mechanisms. Yet, no study has yet performed a high-throughput analysis on the PF after MI and evaluated the subsequent impact on cardiac cells.

Hence, PF of patients that suffered a myocardial infarction are hypothesized to concentrate fibrosis-associated molecules which affects cardiac fibroblast activation and/or differentiation, imparting on myocardial remodelling/dysfunction. In line with this hypothesis, this work aims to evaluate the impact of PF from those patients on the formation of cardiac fibrosis and identify altered molecules with potential to integrate anti-fibrotic therapies for MI. To achieve this, PF and blood samples were collected from two patient cohorts: patient with a recent MI and control patients with stable angina. In brief, the PF after MI was shown to i) accumulate fibrotic markers, namely miR-21, ii) stimulate the differentiation of cardiac fibroblast in myofibroblasts, iii) contain extracellular vesicles capable of internalizing on cardiac fibroblasts and iv) display a different miRNA profiling, compared to the pericardial fluid of stable angina patients, that may regulate cardiac remodelling.

These findings advocate that the content of pericardial fluid changes after MI, namely through the accumulation of miRNAs, impacting of cardiac fibroblasts and consequently is a valuable source to unveil new therapeutic targets to improve remodelling after myocardial infarction.

RESUMO

As doenças isquémicas cardíacas são a principal causa de morte no mundo, sendo responsáveis por 9 milhões de mortes anuais. Dentro destas, o enfarte do miocárdio é uma das mais prevalentes e a principal causa de morbilidade e mortalidade. Recentemente, o líquido pericárdico tem sido considerado como uma potencial fonte de moléculas que podem ser modeladas para promover a regeneração ou reparação do coração enfartado.

Em condições patológicas o líquido pericárdico fica enriquecido em citocinas, fatores de crescimento e hormonas provavelmente secretadas pelas células cardíacas e que, por efeito retrogrado, têm impacto nas células endoteliais, epicardiais e cardiomiócitos. Tanto exosomas como microRNAs, em particular o miRNA-21-5p com propriedades pró-fibróticas, foram também encontrados no líquido pericárdico. Como reservatório de substâncias ativas que afetam o coração, o líquido pericárdico foi recentemente considerado uma fonte privilegiada para estudar mecanismos fisiopatológicos cardíacos. No entanto, nenhuma análise de grande escala molecular foi realizada utilizado o líquido pericárdico após enfarte do miocárdio.

Neste trabalho colocou-se a hipótese de que líquido pericárdico de pacientes que sofreram um enfarte do miocárdio tem uma concentração superior de moléculas associadas à fibrose e que afetam a ativação e/ou diferenciação de fibroblastos cardíacos, e como tal, modelam a remodelagem ventricular. Assim, o objetivo central deste trabalho é elucidar o impacto do líquido pericárdico de pacientes que sofreram enfarte de miocárdio na formação de fibrose cardíaca e identificar moléculas com expressão alterada para integrar novas terapias anti-fibróticas.

Para tal, recolheu-se amostras de sangue e líquido pericárdico de paciente que sofreram um enfarte recente e de pacientes controlo que apresentam um quadro de angina estável. Em suma, foi demonstrou-se que o líquido pericárdico obtido de pacientes de enfarte do miocárdio i) acumula marcadores de fibrose, tais como miR-21, ii) estimula a diferenciação de fibroblastos cardíacos em miofibroblastos, iii) contém vesículas extracelulares capazes de serem internalizados por fibroblastos cardíacos e iv) exibe um perfil de miRNAs diferente quando comparado com o líquido pericárdico de pacientes com angina estável, tem assim potencial para regular a remodelagem cardíaca.

Estes resultados corroboram a hipótese inicial e suportam a utilização do líquido pericárdio para a investigação de novos alvos terapêuticos para melhorar a remodelagem cardíaca após enfarte do miocárdio.

ACKNOWLEDGMENTS

I want to thank Professor Perpétua Pinto-do-Ó for giving me the opportunity to learn and grow in the Stem Cell in Regenerative Biology and Repair group.

I want to show my gratitude to Professor Diana Nascimento for accepting to be my supervisor, for supporting me and having the patience to help me to make sure that this work was a success. Her guidance, expertise and enthusiasm for research were crucial to this accomplishment.

I also thank the group that welcomed right from the start and made all the efforts to make me feel integrated in this family. I thank Vasco and Ana Castanheira for teaching me the basics right from the beginning to make certain that I was doing everything right. I also want to thank Tiago Laundos, Tiago Ramos, Francisca Silva and Tatiana Resend for all the advice and support. I also want to show appreciation to Joana, Márcia and Elsa for all the laughs during the herein thesis. I want to acknowledge Rita for the precious help in the deep sequencing analysis and Francisco for the insight in the statistical analysis of the obtained results.

I want to thank Dr. Rui Cerqueira for the collaborative work and collecting the human samples that made this work possible.

I want to acknowledge the support of i3S scientific platforms (ALM, HEMS, CCGEN, Gencore). Also, I want to show appreciation to Sónia Melo and Cecília Durães for approving the use of the NTA system. Additionally, I want to thank José Henrique and Andreia for all the help regarding the EV labelling and much more and Alexandra Teixeira and Hugo Caires for providing the antibodies and knowledge to perform Western Blot in EV samples.

Queria agradecer todos os meus amigos que sempre me apoiaram em todas as minhas decisões, aos meus amigos de Química e Bioquímica, que mesmo ausentes têm uma presença imensa e aos meus amigos que encontrei em Bioengenharia, que me acompanharam mais de perto nesta reta final do meu percurso académico.

Agradeço imenso à minha família mais chegada, principalmente à minha mãe e a minha irmã por fazerem de tudo para que tivesse sucesso e me motivarem para ser sempre uma pessoa melhor.

Agradeço também à Francisca por me ajudar a superar todas as minhas preocupações e por acreditar em mim independentemente de tudo.

For last but not least, I would like to acknowledge the funding for the herein work, since without it, it would not be possible.

This work was financed by Norte Portugal Regional Operational Programme (NORTE 2020), under the PORTUGAL 2020 Partnership Agreement, through the European Regional Development Fund (ERDF) [NORTE-01-0145-FEDER-000012]; by European Structural and Investment Funds (ESIF), under Lisbon Portugal Regional Operational Programme and National Funds through FCT - Foundation for Science and Technology [POCI-01-0145-FEDER-016385]; by INFARMED – Autoridade Nacional do Medicamento e Produtos de Saúde, I.P. [FIS-FIS-2015-

01_CCV_20150630-157]; and by FCT – Fundação para a Ciência e Tecnologia/Ministério da Ciência, Tecnologia e Inovação in the framework of the project "Institute for Research and Innovation in Health Sciences" [POCI-01-0145- FEDER-007274].

INDEX

LIST OF FIGURES

LIST OF TABLES

ABBREVIATIONS AND SYMBOLS

α-SMA- α-Smooth muscle actin
ACEI- Angiotensin converting enzyme inhibitors
ANP- Atrial natriuretic peptide
ARB- Angiotensin II receptor blocker
BMI- Body mass index
BNP- Brain natriuretic protein
BSA- Bovine serum albumin
CD- Cluster of differentiation
cDNA- Complementary DNA
Da- Dalton
DAMP- Damage-associated molecular patterns
DAPI- 4',6-diamidino-2-phenylindole
DIANA- DNA intelligent Analysis
DMEM- Dulbecco's Modified Eagle's Medium
ECM- Extracellular matrix
ELISA- Enzyme-linked immunosorbent assay
ESCRT- Endosomal sorting complexes required for transport
EV- Extracellular vesicle
FC- Fold change
FDR- False discovery rate
FGF- Fibroblast growth factor
FGM- human fibroblast growth medium
h- hour
HCF- Human cardiac fibroblast
HEPES- 4-(2-hydroxyethyl)-1-piperazineethanesulfonic acid
HRP- Horseradish peroxidase
Hsp- Heat shock protein
IGF-1- Insulin-like growth factor-1
IHD- Ischemic heart disease
IL- Interleukin
KEGG- Kyoto Encyclopedia of Genes and Genomes
LVEF- Left ventricle ejection fraction
MAPK- Mitogen-activated protein kinase
MI- Myocardial infarction
min- minutes
miR- microRNA
MMP- Matrix metalloproteinase
mRNA- messenger RNA
n- number
ns- Non-significant
NTA- Nanoparticle tracking analysis
NYHA- New York Heart association
PBMC- Peripheral blood mononuclear cell
PBS- Phosphate buffer saline
PF- Pericardial fluid
PMN- Polymorphonuclear leukocyte
pri-miR- primary miR
RNA-Seq- RNA sequencing
RT-PCR- Real time-polymerase chain reaction
SD- Standard deviation
secs- seconds
SEM- standard error of the mean
ST2- suppression of tumorigenicity 2
STEMI- ST-segment elevation myocardial infarction
TBS-T- Tris-buffered saline solution with 0.1 % Tween-20
TEM- Transmission electron microscopy
TGF-ß- Transforming growth factor-ß
TMB- 3,3',5,5'-tetramethylbenzidine
TNF-α- Tumor necrosis factor-α
VEGF- Vascular endothelial growth factor

CHAPTER I- INTRODUCTION

1.1. Ischemic Heart Disease

1.1.1. Definition, epidemiology and societal impact

Ischemic heart disease (IHD) designates a group of diseases including unstable and stable angina (*angina pectoris*), sudden cardiac death and myocardial infarction (MI) [1]. This condition is caused by deficient oxygen as a result of ineffective perfusion of oxygenated blood to the myocardium and/or increased cellular oxygen demands [2]. A reduction in oxygen supply is commonly caused by a fixed narrowing, acute rupture or dissection of an atherosclerotic coronary artery but it can also result from coronary artery spasms, embolism or vasculitis, severe anemia or systemic hypotension. On the other hand, ischemia caused by increased oxygen demands can result from sustained tachycardia, uncontrolled hypertension, heart failure and, less frequently, following cardiac revascularization procedures [3].

IHD is the leading cause of death globally, being responsible for almost 9 million deaths annually [4]. While high income countries have seen declines in mortality rates, a reverse trend is observed in lower and middle income countries [5].

Among IHD, MI is the leading cause of morbidity and mortality [6]. MI is defined as myocardial cell death due to prolonged ischemia [7] caused, in the vast majority of cases, by coronary atherosclerotic disease complicated by plaque rupture and subsequent thrombus formation and occlusion of the artery [8].

MI diagnosis relies mostly in electrocardiographic functional alterations, imaging studies and biomarkers of cardiomyocyte death [9]. The most common circulating biomarkers are cardiac troponin I and T (components of the contractile apparatus of cardiomyocytes) and MB fraction of creatinine kinase [7].

According to the American Heart Association, in 2016 15,5 million Americans over 20 years of age showed symptoms of IHD. Moreover, the prevalence of this disease increases with age and estimates indicate that an American will suffer a MI approximately every 42 seconds, [10]. In the USA, annual costs of IHD reach 188 billion dollars and is projected to increase up to 366 billion dollars by 2035 [11].

In Europe, IHD is also the leading cause of death, being responsible for 1,74 million deaths per year. In 2015, 3 million new cases of IHD were reported [12].

1.1.2. Pathophysiology and current treatments

Following coronary occlusion, aerobic metabolism stops immediately, resulting in rapid ATP depletion and accumulation of metabolites. For short periods of ischemia (less than 15 to 20 minutes), metabolic alterations are fully reversed once coronary flow is reestablished, allowing cardiomyocyte survival [9].

In contrast, long periods of ischemia result in permanent damage to the heart, namely, sarcolemma disruption (small breaks in the plasmalemma and formation of subsarcolemmal blebs) and perturbations of the mitochondrial architecture (severe mitochondrial swelling, disorganized cristae, and ultrastructural evidence of amorphous matrix densities) [9].

Following MI, the heart initiates a reparative process characterized by an inflammatory, a proliferative and a final maturation phase, which partially overlap (**Figure 1**). Because the adult human heart does not effectively regenerate, this cascade of events results in the formation of a non-contractile collagenous scar to replace lost cardiomyocytes [13].

The inflammatory phase is characterized by the activation of innate immune cells after detection of damage-associated molecular patterns (DAMPs, danger signals or alarmins) that are released by necrotic cells [14]. The high mobility group box 1 is a crucial alarmin produced following MI, signaling through the receptor for advanced glycation end products, toll-like receptors and matrix metalloproteinase (MMP) enzymes [15]. The detection of alarmins combined with the release of reactive oxygen species and activation of the complement cascade will result in the upregulation of chemokines, proinflammatory cytokines and adhesion molecules. This molecular milieu potentiates leukocyte recruitment to the injured myocardium, supporting extracellular matrix (ECM) remodeling and clearance of dead cells [9].

The proliferative phase begins once proinflammatory stimuli from dead cells is reduced. This stage is characterized by an decrease in the frequency of proinflammatory leukocytes, whereas fibroblasts, myofibroblasts (activated fibroblasts) and vascular cells increase their frequency in response to secretion of cytokines and growth factors (e.g. fibroblast growth factor (FGF)-2, angiotensin II, platelet-derived growth factors and mast cell-derived tryptase and chymase) [9, 16].

In addition, ECM plays an important role in this process, as matricellular proteins transduce key activating signals in fibroblasts, macrophages and vascular cells [17]. Myofibroblasts become the dominant cell type in the infarcted myocardium as a result of transforming growth factor β (TGF-β)-induced differentiation of fibroblasts [16]. Myofibroblasts are phenotypically different from fibroblasts, exhibit contractions and express α-smooth muscle actin (α-SMA) [18]

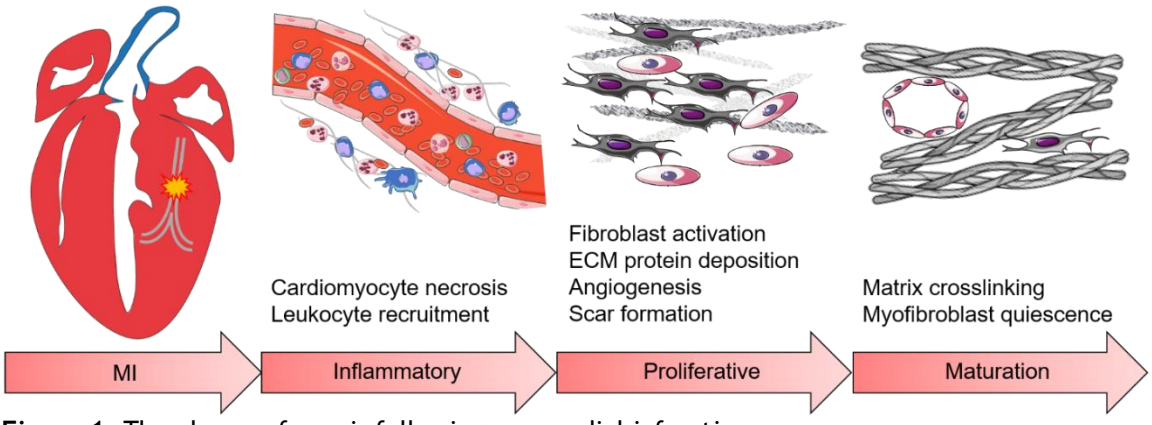

Figure 1: The phases of repair following myocardial infarction

These cells secrete large amounts of structural matrix proteins (such as collagens and fibronectin), but also deposit matricellular proteins and modulate matrix metabolism by expressing MMPs and their inhibitors, forming a scar in the infarcted myocardium [16].

The last stage begins with the maturation of structural matrix proteins deposited in the injury site (e.g. collagen crosslinking). At this time, myofibroblasts enter in a quiescent state characterized by diminished expression of matricellular proteins [9]. The signaling pathways that regulate this process are still poorly understood but the removal of stimulatory fibrogenic growth factors, clearance of matricellular protein and activation of intracellular STOP signals may contribute to the latter [9].

These molecular, cellular and interstitial changes are accompanied by changes in size, shape and function of the heart as a consequence of MI, which overall are designated "cardiac remodeling" [19]. At the morphological level, cardiac remodelling is characterized by dilation of the infarcted area during acute phase of MI and eccentric hypertrophy in the chronic phase. The initial remodeling phase after MI has been considered beneficial, leading to clearance of necrotic and to scar formation, however, progressive remodeling becomes deleterious and associated with a poor prognosis [20].

The current practice to treat patients that suffered a MI is reperfusion of the ischemic myocardium by percutaneous coronary intervention [21]. After this acute phase, several measures can be applied to reduce the risk of complications, including: 1) changes in lifestyle (smoking cessation, healthy diet, blood pressure control and exercise-based programs), 2) administration of anti-thrombotic drugs such as aspirin and $P2Y_{12}$ inhibitors, 3) administration of ß-blockers, 4) lipid-lowering therapy using statins, 5) administration of angiotensin-converting enzyme inhibitors and angiotensin receptor blockers and 6) the use of mineralocorticoid/aldosterone receptor antagonists [21].

As mechanisms underlying cardiac response to MI are becoming progressively revealed, new windows of opportunity become available for therapeutic exploitation. Therapies may target the acute phase of MI with the purpose of minimizing cardiomyocyte death. For example focusing on ischemia preconditioning, inhibition of oxidative stress, attenuation of calcium overload, correction of pH, suppression of pro-apoptotic pathways and activation of pro-survival pathways [9]. Alternatively, the therapeutic strategy may also address the chronic stage of MI, modulating inflammatory and/or fibrotic responses [9].

In the past years experimental studies have focused on cardiac regenerative potential, since the neonatal mouse was shown to regenerate after apical resection at post-natal day 1 [22]. This report, despite recent controversy and accumulation of studies showing only a limited regenerative capacity [23], has revolutionized the cardiovascular field by proposing an injury-model to unveil mechanisms underlying mammalian heart regeneration, which could be further employed to develop novel therapies to treat MI in the adult human heart.

1.2. Pericardium and Pericardial Fluid

1.2.1. Development, Anatomy and Physiology

The pericardium is a roughly flask-shaped sac that contains the heart and proximal portions of the great vessels [24]. In humans, the pericardium is located inside the middle mediastinum posteriorly to the sternum and the cartilages of the third to seventh left rib [25]. The pericardial sac is constituted by an external fibrous connective tissue layer, the fibrous pericardium, and an internal visceral wall denominated serous pericardium (**Figure 2**) [25]. The latter consists of a single continuous layer of mesothelium that coats the fibrous layer and extends over the root of the great vessels to completely cover the external surface of the heart (also known as epicardium) and also the lateral sides of the *venae cavae* and the anterior portion of the pulmonary veins [24]. The pericardial cavity is filled with a serous fluid named pericardial fluid (PF) that lubricates the visceral pericardium and the epicardium since, in every heartbeat, these membranes glide over each other [26].

The pericardium has several important functions such as lubricating the moving surfaces of the heart, stabilizing its anatomical position and isolating it from adjacent anatomical structures. The pericardium also 1) reduces endomyocardial tension by limiting heart dilation during diastole, 2) prevents cardiac hypertrophy in pressure overload conditions, 3) reduces the right ventricular impulse work in left ventricular overload conditions, 4) prevents retrogression of ventriculoatrial blood during high end-diastolic ventricular pressures, 5) maintains a negative endothoracic pressure which is crucial for atria blood filling, 6) influences nervous stimulation and 7) contributes to the formation of a hydrostatic compensation system ensuring that end-diastolic pressure remains the same at all hydrostatic levels [25].

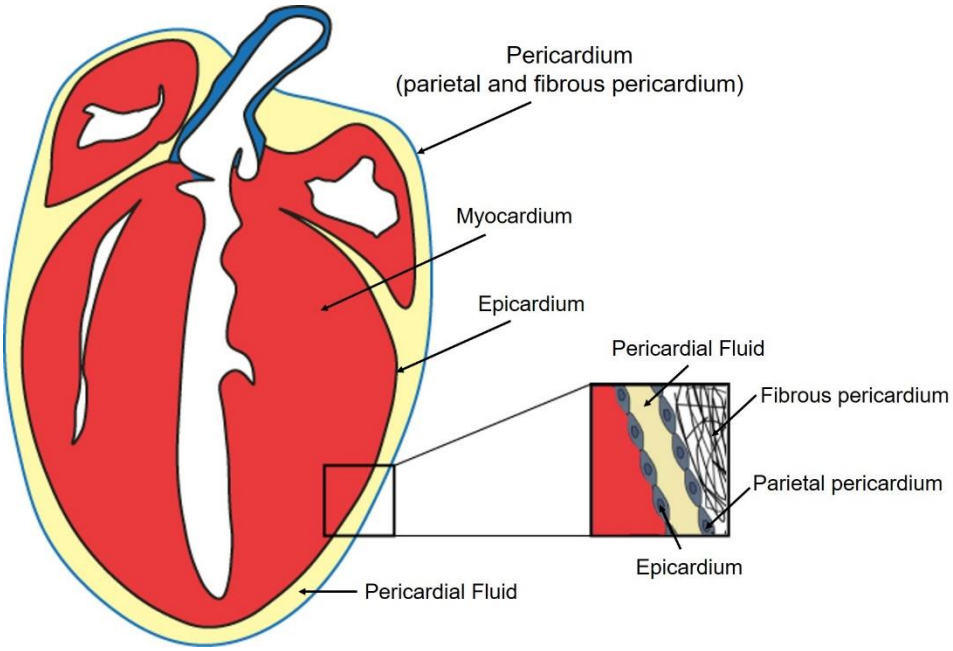

Figure 2: Schematic representation of the pericardial layers and layers of the heart wall.

The development of the pericardium in humans occurs during the fourth week of embryogenesis. In this phase, the intraembryonic coelom gives rise to 3 body cavities: the pericardial cavity, peritoneal cavity, and two pleuropericardial canals. Each cavity would contain a parietal and visceral layer that are lined with a mesothelium layer derived from the mesoderm. The pericardial and peritoneal cavities are separated by the growth of the septum transversum, the primordium of the central tendon of the diaphragm. As the bronchial bud grows, the pleuropericardial canals separate the pleural cavities from the pericardial cavity. The pleuropericardial membrane later becomes the fibrous pericardium [27].

1.2.2. Function and Content of the Pericardial Fluid

The adult human pericardium contains in average 15-35 mL of PF [25], which is considered a passive ultrafiltrate of plasma [28].

As an ultrafiltrate of plasma, PF shares some of the components with its origin such as Na^+, K^+ and Cl^- [28]. PF also contains other molecules which concentration is approximately equal to plasma such as glucose, urea, creatinine and uric acid, whereas the lactate dehydrogenase and protein levels are above values reported for other plasma ultrafiltrates [29].

The PF has also been shown to contain an heterogeneous population of cells with the presence of mesothelial cells, lymphocytes, granulocytes, macrophages, eosinophils and basophils [25].

PF composition can also be enriched in several mediators produced by the cardiac tissue such as cytokines, growth factors and hormones [30]. The production of this molecules can be altered depending on the health condition of the patient [31].

More recently, extracellular vesicles (EVs) have also been identified in PF [32]. EVs refers to different populations of vesicles that include apoptotic vesicles, microvesicles and exosomes [33]. These populations have different attributes as in size, density, biogenesis, content and biomarkers (**Table 1**).

The specific EVs that were described in the PF were exosomes that are particles that range from 30-100 nm in diameter, have a density of 1,10–1,18 g/mL and may contain all known molecular constituents of a cell, such as proteins, RNA, microRNAs (miRs) and DNA [34].

Exosomes are originated by the endolysosomal pathway (**Figure 3**) in which the early endosomes fuse with endocytic vesicles and incorporate their content into those destined for recycling, degradation or exocytosis. From this process, late endosomes arise and can be characterized by the presence of multiple interluminal vesicles. After that, exosomes are released through the fusion of late endosomes to the plasma membrane [35]. Several biomarkers can be used to detect exosomes for instance, proteins from the tetraspanins family (TSPAN19, TSPAN30, cluster of differentiation (CD) 81, CD82, CD9, CD63), endosomal sorting complexes required for transport (ESCRT) proteins (Alix, TSG101), actin, flotillin, Heat shock cognate 70, Heat shock protein (Hsp) 90, Hsp60, Hsp20, clathrin and integrins [34].

Table 1: Classification and characteristics of different types of EVs.

	EXOSOMES	MICROVESICLES	APOPTOTIC BODIES
SIZE	30-100 nm [33]	100-1000 nm [36]	500-5000 nm [34, 37]
DENSITY	1,13-1,19 g/mL [34]	1,04-1,07 g/mL [34]	1,16-1,28 g/mL [34]
BIOGENESIS	Inward luminal budding of the membrane and fusion of multivesicular bodies with the cell membrane [34]	Outward budding of the cell membrane through calpain activation, calcium influx and cytoskeleton reorganization [36]	Outward budding of the cell membrane of apoptotic cells [37]
COMPOSITION	Higher levels of aminophospholipids and lipid ceramide compared to the outer leaflet of the plasma membrane [34]	Similar to that of the cell membrane but without asymmetric distribution of lipids [34]	Externalization of phosphatidylserine but distributed on the cell surface and presence of Annexin I and calreticulin [34]
CONTENTS	mRNA, miR, other non-coding RNA, cytoplasmic and membrane proteins, major histocompatibility complex (MHC) [33, 34]	mRNA, miR, other non-coding RNA, cytoplasmic and membrane proteins [33]	Nuclear fractions, DNA, cell organelles [34]
BIOMARKERS	Tetraspanins (CD61, CD81, CD82, CD9, TSPAN29, TSPAN30), ESCRT proteins (Alix, TSG101), Flotillin 1 and Flotillin 2, Hsp70, Hsp90, Hsp60 and Hsp20 [33, 34]	Annexin V, Integrins and CD40 ligand [33]	Annexin V and phosphatidylserine [33]

Exosome signaling has been shown to influence central processes of cardiac remodeling [38] such as angiogenesis [39] and cardiac fibrosis [40], therefore, the study of this vesicles and their cargo is important for improving understanding of myocardial-injury response.These vesicles are known to carry miRs, which are non-coding RNAs composed by 21-22 nucleotides that influence messenger RNA (mRNA) translation or decay [41].

Mammalian miRs can be classified as canonical and non-canonical depending on their biogenesis. In the canonical pathway, miR genes are transcribed producing primary miR (pri-miR) transcripts, resulting in a long sequence that may contain modifications identical to those present in mRNAs and pre-mRNAs [42]. Following transcription, pri-miRs are cleaved by Drosha bound by its DiGeorge chromosomal region 8 subunit producing a harpin structured precursor

denominated pre-miR that is exported to the cytoplasm by Exportin5 [43]. Then, the pre-miR is cleaved by Dicer, producing a miR duplex intermediate which will bind to an Argonaute protein, incorporating the mature miR and discarding the other strand [42]. The miR-bounded Argonaute will then bind to their target mRNAs through imperfect base pairing, although nucleotides 2 to 7 (the seed sequence) are generally complementary to target sites that can trigger translational repression and/or target mRNA destabilization in multiprotein complexes that include GW182 proteins, deadenylases, and poly(A) binding proteins [44].

Non-canonical miRs differ from canonical in the fact that their processing does not require all the protein factors mentioned previously [45]. Such RNAs can be defined as endogenous small interfering RNAs [42]. This small RNAs have also been shown to be involved in cardiac remodeling following MI [46].

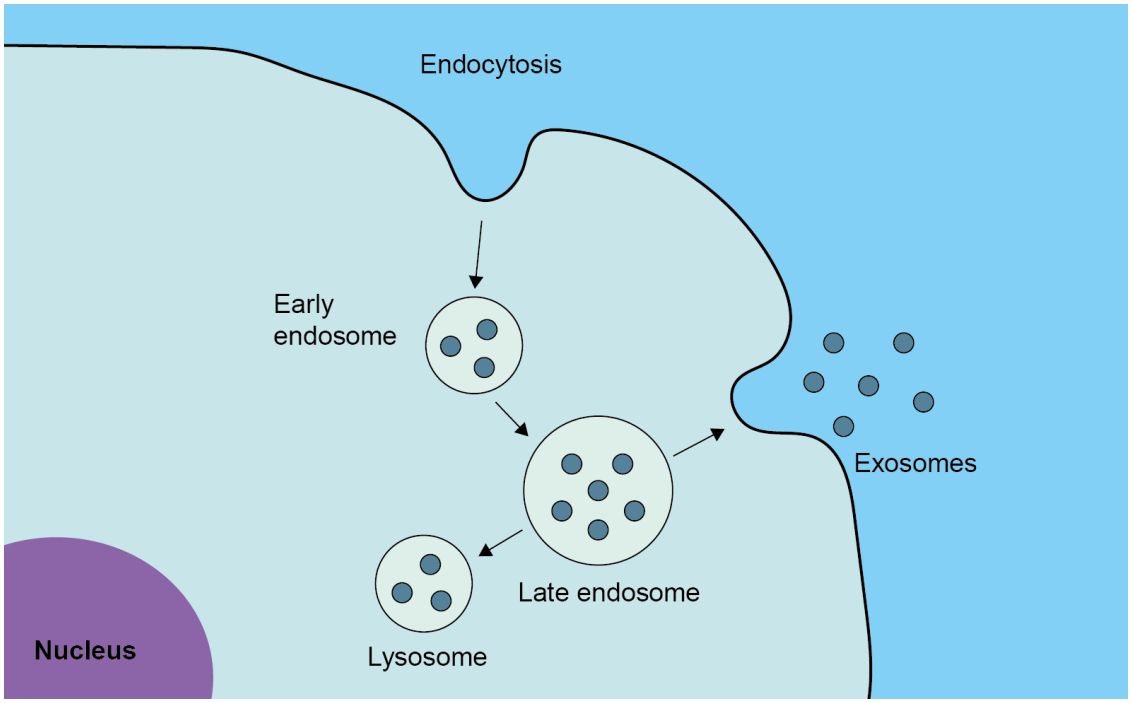

Figure 3: Biogenesis and release of exosomes

1.2.3. Pericardial Fluid Biochemical Alterations in disease

As mentioned above, PF content becomes altered in case of cardiac injury or disease (**Table 2**). In earlier studies regarding alteration in disease, patients with unstable angina were shown to have higher concentrations of growth factors responsible for the promotion of angiogenesis [30] such as vascular endothelial growth factor (VEGF) and acid and basic fibroblast growth factor (FGF-1 and FGF-2) compared to controls [47-51]. This data is conflicting with another study reporting vascular endothelial cell apoptosis when F2 cells, a mouse vascular endothelial cell line, were cultured with PF from patients with unstable angina [31]. Also, IL-1ß levels were shown to be increased in PF from unstable angina patients compared to MI and

stable angina patients. The same trend was seen in serum from the same patients with similar concentrations [52].

Regarding patients with MI, PF showed increased levels of MMP-2, MMP-9, interleukin (IL)-8 and polymorphonuclear leukocyte (PMN) elastase [53, 54]. These MMPs and PMN elastase are expressed by macrophages and neutrophils in the infarcted site [53], supporting the involvement of PF in inflammatory signaling after ischemic injuries. This study complements an earlier one in which PF from patients with MI contained greater levels of IL-2R, IL-6 and tumor necrosis factor-α (TNF-α) compared to stable and unstable angina groups [52].

Insulin-like growth factor-1 (IGF-1) was also detected in PF and had altered levels in the PF of patients with left ventricular dysfunction and heart failure [55]. This growth factor has been shown to improve cardiac function after MI by stimulating contractility and promoting tissue remodeling [56]. Brain natriuretic protein (BNP) and atrial natriuretic peptide (ANP) levels were also analyzed in the PF fluid of MI patients and the concentrations of those peptides were higher in PF compared with plasma, regardless of MI injury site [57]. BNP levels were elevated in MI patients, functioning as a predictor of short- and long-term mortality and show an interaction between cardiac and renal function after MI [58]. ANP was also elevated in MI patients compared to control patients and was shown to improve cardiac function and mechanical efficiency of patients that suffered a prior MI, possibly by activation of a pathway that directly affects oxidative phosphorylation in the mitochondria of cardiomyocytes [59].

FGF-2 was detected in higher levels in PF compared to serum and data suggested that this growth factor is a major determining factor in normal myocyte growth [60]. This growth factor promotes cardiac hypertrophy and fibrosis by activating mitogen-activated protein kinase (MAPK) signaling [61]. The MAPK signaling pathway has been shown to be involved in the induction of myocardial cell apoptosis. Iwakura, A., et al. shown that PF from patients with IHD induced apoptosis in primary cardiomyocyte cultures by activation of an oxidant stress-sensitive p38 MAPK pathway [62].

More recently, research has been focusing mainly in the presence of exosomes and miR in the PF. Kuosmanen SM, et al. profiled miRs from patients with several heart diseases, such as MI, mitral valve insufficiency, aortic stenosis, aortic valve insufficiency and other cardiovascular disease [41]. Although this study was unable to detect differences in the miR content amongst different cardiovascular diseases, it presented an extended list of miRs abundant in the PF. The most abundant miRs were miR-21–5p, miR-451a, miR-125b-5p, let-7b-5p and miR-16–5p [41]. MiR-21 is highly expressed in the cardiovascular system, predominantly in cardiac fibroblasts [63], is involved in fibrotic remodeling after MI [46] and promotes cardiomyocyte hypertrophy [41]. MiR-451, has been shown to be protective against ischemic damage of the myocardium and is upregulated in human hearts after MI [64]. Concerning miR-125b, it has been shown to protect the myocardium from ischemia/reperfusion injury by decreasing up to 60% the infarct size and appears to have lower levels in the plasma of MI patients compared to controls [41, 65]. Let-7b-5p belongs to the let-7 family which is also highly expressed in the cardiovascular system and plays an active role in the pathogenesis of MI and heart failure [66]. Finally, miR-16–5p has been shown to have unaffected circulating levels in

patients with heart failure [67], but is increased in plasma of rats with hypertension-induced heart failure, compared with controls [68]. PF has also been shown to be enriched with miR-423-5p compared to serum particularly in patients with unstable angina [69].

Regarding PF-isolated EVs, Beltrami and colleagues have shown that the latter were able to potentiate the angiogenic capacity of endothelial cells *in vitro* through mechanisms partially mediated by let-7b-5p [70]. In addition, clusterin, present is EVs of the PF obtained from patients with MI influences arteriogenesis, epicardial activation (discussed in section 3) and apoptosis [32].

Table 2: Growth factors detected in PF of patients and their alteration regarding disease

Disease	Changes in growth factors	References
Unstable angina	↑FGF-1 in PF compared to non-IHD patients and serum from the same patients ↑FGF-2 in PF compared to non-IHD patients and plasma from the same patients ↑VEGF in PF of class III unstable angina compared to class I or II unstable angina, stable angina and non-IHD patients ↑IL-1β in PF compared MI and stable angina patients	[47-51]
MI	↑MMP2 in PF compared to stable angina patients and plasma of remodeling and non-remodeling patients ↑MMP9 in PF compared to stable angina patients ↑IL-8 in PF compared to stable angina patients and serum from MI, stable and unstable angina patients ↑PMN elastase in PF compared to stable angina patients ↑IL-2R in PF compared to stable and unstable angina patients and serum from the same patients ↑TNF-α in PF compared to stable and unstable angina patients and serum from the same patients ↑IL-6 in PF compared to stable and unstable angina patients and serum from the same patients ↑ANP in PF of anterior MI patients compared to posterior MI and no MI patients and plasma from the same patients ↑BNP in PF of anterior MI patients compared to posterior MI patients and no MI patients and plasma from the same patients	[52-54, 57]
Heart failure	↑IGF-1 in PF of heart failure patients but decreased in plasma from the same patients ↑BNP in PF of NYHA class III patients compared to NYHA class I and II patients and plasma from the same patients	[55, 71]

NYHA-New York Heart Association

1.3. Pericardial Fluid as a Source of Therapeutic Targets and Biomarkers of Disease

Following the before mentioned biochemical alterations, one can conclude that the PF mediates important cellular functions in response to injury and, thus, is a potential candidate for further studies aiming at the identification of therapeutic molecules.

The therapeutic potential of the PF has been demonstrated resorting to experimental animal models. In 2010, Beltrami and colleagues injected PF from infarcted patients in the pericardial cavity of non-infarcted mouse hearts, resulting in the proliferation of epicardial cells which reactivated a developmental-like expression program [72]. More recently a high-throughput analysis of exosomes collected from MI patients revealed the presence of clusterin. In the same work, the therapeutic potential of clusterin in MI setting was tested in a mouse model of the disease. Clusterin showed a protective effect on cardiomyocytes, decreased apoptotic events and activated epithelial to mesenchymal transition of epicardial cells. Importantly, this treatment improved cardiac function after MI, as determined by hemodynamic studies [32].

Another example of the valuable interest of PF is the detection of biomarkers of cardiac ischemia. Hence, it has been showed that cardiac troponin I levels following myocardial injury are higher in PF compared with serum, endorsing PF as a valuable source of novel biomarkers that can be easily overlooked in the plasma owing to lower concentrations [73]. Recently, the cardiovascular community has been devoted to replacing troponins as biomarkers by miRs which can be easily detected by real time-polymerase chain reaction (RT-PCR) technique [46, 74]. As it has been shown that PF is particularly rich in miRs, high-throughput analysis of PF in different disease scenarios, presently lacking in the field, are expected to provide new markers for early detection of cardiac diseases.

AIMS

Classically the pericardial fluid (PF, liquid surrounding the heart) was viewed as the lubricant protecting the heart [26]. However, in pathological conditions the PF becomes enriched in cytokines, growth factors and hormones likely secreted by cardiac cells, which by retrograde effect impact on vascular, epicardial cells and cardiomyocytes [31, 39]. Exosomes and microRNAs, in particular pro-fibrotic miRNA-21-5p, were also found in PF. As reservoir of active substances that affect the heart, PF has been recently considered a privileged source to investigate cardiac pathophysiologic mechanisms. Yet, no study has yet performed a high-throughput analysis on the PF after MI and evaluated the subsequent impact on cardiac cells.

Our **working hypothesis** is that the PF of patients that suffered a MI concentrates fibrosis-associated molecules which affects cardiac fibroblast activation and/or differentiation, imparting on myocardial remodelling/dysfunction. Hence, the **broad aim** of this Master thesis is to evaluate the impact of PF from those patients on the formation of cardiac fibrosis and identify altered molecules with potential to integrate anti-fibrotic therapies for MI. To achieve this, PF and blood samples were collected from two patient cohorts: patient with a recent MI and control patients with stable angina.

The **specific aims** of this Master thesis were:

- Quantify cardiac fibrosis markers in PF and plasma samples;
- Evaluate the impact of PF on the activation of human cardiac fibroblasts *in vitro*;
- Quantify cardiac fibrosis-related miRs in PF and plasma samples;
- Identify differently expressed miRNAs in PF of MI and stable angina patients;
- Isolate and characterize EVs from PF and plasma samples from MI and stable angina patients;
- Determine if EVs from the PF are internalized by cardiac fibroblasts;

CHAPTER II – MATERIALS AND METHODS

2.1. Sample collection and processing

Peripheral blood and pericardial fluid (PF) were collected from two patient cohorts undergoing coronary artery bypass grafting: i) a control, stable coronary artery patients (stable angina, without previous MI or acute coronary syndrome) and ii) a MI group, composed of patients with a recent first MI episode (maximum 3 months before surgery). The two groups were characterized in terms of age, sex, age, cardiovascular risk factors and medication at the time of surgery (**Table 3 and 4**).

Within two hours after blood (using EDTA as anti-coagulant) and PF collection samples were processed as follows. PF was centrifuged at 1200 *x g* for 10 minutes (min) at room temperature without brake and acceleration and the cellular fraction of the PF was separated from the liquid fraction. PF cells were incubated with 5 mL red blood cell lysis buffer (10 mM Tris-base, 150 mM NH_4Cl) for 8 min at 37 ºC, the tube was is then filled with PBS and centrifuged at 300 *x g* at 10 min. The cell pellet was resuspended in 500 µL of TRIzol (ThermoFisher Scientific) and stored at -80 ºC. PF was centrifuged twice at 2500 *x g* for 15 mins without brake and acceleration at room temperature and the supernatant was stored at -80 ºC in 1 mL aliquots.

Regarding peripheral blood, plasma was separated from the buffy coat by centrifugation at 1200 *x g* for 10 min at room temperature without brake and acceleration. Plasma was stored at -80 ºC in 1 mL aliquots. PBS was added to the buffy coat up to 7 mL and peripheral blood mononuclear cells (PBMCs) were separated using Lymphoprep™. Briefly, the diluted buffy coat was transferred to the top of 4 mL of Lymphoprep™ and centrifuged at 400 *x g* for 30 minutes without brakes and acceleration. After that, PBMC layer were collected and centrifuged at 300 *x g* for 8 mins and the pellet is resuspended in 500 µL of TRIzol (Thermo Fisher Scientific) and stored at -80 ºC

2.2. EVs isolation

EVs were isolated from plasma and PF from both patient cohorts by ultracentrifugation. Briefly, plasma or PF were centrifuged twice at 2500 *x g* for 15 mins at room temperature and diluted in equal volume of filtered PBS. Then samples were filtered by gravity through a 0,8 µm filter (Millipore) and centrifuged at 12600 *x g* for 30 mins at 4 ºC. The supernatant was collected and centrifuged at 100000 *x g* for 70 min at 4ºC. Supernatant was collected and stored at -80 ºC as a control and EV pellet was resuspended with filtered PBS and centrifuged again at 100000 *x g* for 70 mins at 4ºC. The EV pellet was resuspended in 100 µL of filtered PBS and stored at -80 ºC. Ultracentrifugation was performed in an Optima XE-100 Ultracentrifuge (Beckman Coulter) with a Type 70 Ti Rotor and 26,9 mL Quickseal tubes.

Table 3: Patient demographic data and cardiovascular risk factors

	Control (n=6)	MI (n=24)	p-value
Age (years)	66,2±10,4	68,6±8,0	ns
Female (%)	1 (16,67)	2 (8,33)	ns
STEMI (%)	-	5 (20,83)	
LV EF (%)	58,83±3,37	45,88±13,70	0,030
IHD Risk Factors			
BMI ($Kg.m^{-2}$)	28,28±2,61	27,07±3,55	ns
Diabetes mellitus (%)	2 (33,33)	15 (62,50)	ns
Hypertension (%)	4 (66,67)	20 (83,33)	ns
Dyslipidemia (%)	6 (100,0)	19 (79,17)	ns
Smokers (%)	1 (16,67)	5 (20,83)	ns
Ex-smokers (%)	2 (33,33)	9 (37,50)	ns
Previous IHD (%)	0 (0,00)	4 (16,67)	ns

Continuous variables are presented as mean±standard deviation (SD). n-number; STEMI–ST-segment elevation myocardial infarction; LV EF-left ventricle ejection fraction; BMI-body mass index

Table 4: Patient medication data

	Control (n=6)	MI (n=24)	p-value
Aspirin (%)	3 (50,00)	13 (54,17)	ns
ß-blockers (%)	5 (83,33)	11 (45,83)	ns
Statins (%)	5 (83,33)	17 (70,83)	ns
ACEI (%)	3 (50,00)	7 (29,17)	ns
Antidiabetics (%)	2 (33,33)	13 (54,17)	ns
Fibrates (%)	0 (0,00)	3 (12,50)	ns
Ca^{2+} Channel Blockers (%)	2 (33,33)	4 (16,67)	ns
Antiaggregant (%)	1 (16,67)	6 (25,00)	ns
Nitrates (%)	2 (33,33)	6 (25,00)	ns
ARB (%)	0 (0,00)	6 (25,00)	ns
Spironolactone (%)	0 (0,00)	3 (12,50)	ns
Bronchodilators (%)	1 (16,67)	3 (12,50)	ns
Anticoagulants (%)	1 (16,67)	2 (8,33)	ns
Corticosteroids (%)	1 (16,67)	2 (8,33)	ns

ACEI-Angiotensin converting enzyme inhibitors; ARB-Angiotensin II receptor blocker

2.3. EVs characterization

The isolated EVs were characterized by size, particle concentration and protein content by the methods described below.

2.3.1. Transmission Electron Microscopy (TEM)

TEM allows the visualization of EVs, confirming the efficacy of the isolation. To accomplish that, 5 µL of fresh samples were mounted on Formvar/carbon film-coated mesh nickel grids (Electron Microscopy Sciences, Hatfield, PA, USA) and left standing for 2 min. The liquid in excess was removed with filter paper, and 10 µL of 1% uranyl acetate were added on to the grids and left standing for 10 secs, after which, liquid in excess was removed with filter paper. Visualization was carried out on a JEOL JEM 1400 TEM at 120 kV (Tokyo, Japan). Images were digitally recorded using a CCD digital camera Orious 1100W Tokyo, Japan at the HEMS / i3S of the University of Porto.

2.3.2. Nanoparticle Tracking Analysis (NTA)

NTA allows the characterization of EVs regarding their size and particle concentration. Five µL of resuspended EVs or UC controls were diluted 1:200 in filtered PBS (final volume of 1 mL) and, following homogenization, the dispersion was injected into a Nanosight NS300 system (Malvern Instruments, U.K.). The equipment captured 3 shorts videos (30 secs) with all camera settings fixed on all measurements. This instrument then uses light scattering and Brownian motion properties to obtain size and particle concentration.

2.3.3. Western Blot (WB)

EVs were concentrated by speed vacuum and lysed with Winman's buffer (1% NP-40; 0,1 M Tris-HCl pH 8,0; 0,15 M NaCl and 5 mM EDTA) complemented with EDTA-free protease and phosphatase inhibitor cocktail (Roche). This mix was shaken for 30 min at 4 ºC, heated at 95 ºC for 10 min and stored at -20 ºC. The Bio-Rad DC™ Protein assay was used for protein quantification with appropriate bovine serum albumin (BSA) standards to generate a standard curve and PBS as a blank control. After 15-30 min of incubation with the assay reagent in the dark, absorbance was read at 655nm.

Following protein quantification, 3-7 µg of protein in EVs was mixed with loading buffer (Tris-HCl 1 M, 5% SDS, 12% Glicerol, 12% ß-mercaptoethanol and 0.024% bromophenol blue), boiled for 5 min at 95ºC (for protein denaturation) and separated on 10% Tris-glycine SDS-Page polyacrylamide gels at 70 V (for at least 30 min) during approximately 1 h and 30 min at 100 V. This separation was done using a running buffer prepared from a commercial 10x Tris/Glycine/SDS buffer solution (Bio-Rad). Proteins were then transferred to a nitrocellulose membrane (Amersham Protran 0.45 NC, GE Healthcare) for approximately 2 h at 100 V using transfer buffer prepared from a commercial 10x Tris/Glycine buffer solution (Bio-Rad) to which 20% of methanol was added. These procedures were done in a Bio-Rad Western Blot System.

Membranes were stained with Ponceau S solution (Sigma-Aldrich, Co.) to confirm efficient transfer. Membranes were blocked in a Tris-buffered saline solution with 0.1 % Tween-20 (Promega) (TBS-T) with 5% (w/v) non-fat dry milk (Molico) for 2 h at room temperature. Membranes were incubated with primary antibodies, which were prepared in blocking solution, for 1 h and 30 min at room temperature or overnight at 4 ºC, washed 3 times in TBS-T during 10 min with agitation and, finally, incubated with the correspondent secondary antibodies for 1 h at room temperature.

The antibodies used and respective dilutions were: anti-Alix (sc-49268) 1:400, anti-Flotillin-1 (sc-74567) 1:1000, anti-Syntenin-1 (sc-100336) 1:200 and anti-Cytochrome C (sc-13560) 1:1000 , from Santa Cruz Biotechnology and anti-CD63 (EXOAB-CD63A-1) 1:500, anti-CD81 (EXOAB-CD81A-1), 1:500 and anti-Hsp70 (EXOAB-Hsp70A-1) 1:500, from System Biosciences. The following secondary antibodies were used: donkey anti-goat IgG-HRP (sc-2020) 1:2000 and goat anti-mouse IgG-HRP (sc-2031) 1:2000, from Santa Cruz Biotechnology and goat anti-rabbit HRP (included in the references of the primary antibodies from the same company) 1:20000 from System Biosciences. Membranes were washed 3 times in TBS-T for 10 min and the signal was detected using ECL Western Blot Detection Reagents (GE Healthcare), the chemiluminescence Amersham Hyperfilm ECL (GE Healthcare) and the Kodak GBX developer and fixer (Sigma-Aldrich, Co.).

2.4. MiR quantification

2.4.1. RNA extraction

RNA extraction from plasma and PF samples (200 µL) was performed using the miRNeasy® Serum/Plasma Kit (QIAGEN) following manufacturer instructions. During extraction 3,5 µL of spike-in (ce-miR-39) at 1,6 x 10^8 copies/µL was added to the mixture. RNA was stored at -80 ºC. RNA quantity and quality were assessed using a NanoDrop™ 1000 Spectrophotometer (ThermoFisher Scientific). The absorbance at 260 nm was used to calculate RNA concentration and ratios 260/280 and 260/230 nm measured contamination with proteins and phenols, respectively.

2.4.2. Reverse transcription

For complementary DNA (cDNA) production, the miScript® II RT Kit (QIAGEN) was used following the manufacturer's protocol. Briefly, a master mix containing was prepared according to **Table 5** before incubation at 37 ºC during 60 min in a thermocycler. After that, the mix was incubated at 95 ºC for 5 min and cDNA stored at -20 ºC.

Table 5: Reverse transcription master mix components.

Component	Volume/reaction
5x miScript HiSpec Buffer	4 µL
10x miScript Nucleics Mix	2 µL
miScript Reverse Transcriptase Mix	2 µL
TRNA	12 µL
Total volume	20µL

2.4.3. Real-time PCR (RT-PCR)

To quantify miR expression, RT-PCR was performed using the miScript® SYBR Green PCR Kit (Qiagen). A master mix has been prepared without cDNA as shown in **Table 6**. The reaction mix is then added to a 96-well PCR low plate and centrifuged at 1000 *x g* for 1 min. The cDNA was then added to the wells and centrifuged again at 1000 *x g* for 1 min. Wells were covered by a sealing tape to prevent evaporation of the reaction mix, the plate was centrifuged at 1000 *x g* for 1 min and placed in a CFX96 Touch™ Real-Time PCR Detection System (Biorad). The programmed PCR cycling is detailed in **Table 7**. The primers assays used were the following: Hs_miR21_2 (21830; MS00009079), Hs_miR-29a-1 (218300; MS00003262), Hs miR-29c_1 (218300; MS00003269) from QIAGEN.

Table 6: RT-PCR reaction mix components

Component	Volume/reaction
2x QuantiTect SYBR Green PCR Master Mix	5 µL
10x miScript Universal Primer	1 µL
10x miScript Primer Assay	1 µL
RNase-free water	2 µL
cDNA	1 µL
Total volume	10 µL

Table 7: RT-PCR cycling conditions (*Fluorescence data collection is performed in this step every cycle)

Step		Time	Temperature
3-step cycling (40 cycles)	Activation	15 min	95 ºC
	Denaturation	15 secs	94 ºC
	Annealing	30 secs	55 ºC
	Extension*	30 secs	70 ºC

2.5. Cardiac fibrosis markers quantification

An enzyme-linked immunosorbent assay (ELISA) kit was used to detect and quantify human interleukin(IL)-1 receptor 4 /suppression of tumorigenicity 2 (ST-2) (RayBio®) in PF and plasma samples of MI and control patients.

Biological samples and standards were incubated in sealed wells for 2 hours (h) and 30 min, after which they were washed and added a previously prepared biotinylated antibody solution and incubated for 1h. Wells were washed and incubated 45 min with a horseradish peroxidase (HRP)-coupled streptavidin solution. Wells were washed once again and incubated with a 3,3',5,5'-tetramethylbenzidine (TMB) solution for 30 min. This step yields a blue color, caused by the oxidation of TMB as a result of the hydrolysis of hydrogen peroxide by HRP. To stop the before-mentioned reaction, a solution containing sulfuric acid was added to the wells after incubation, changing the color of the solution to yellow. The absorbance was then read immediately at 450 nm.

All incubations in the were done at room temperature and in slight agitation.

2.5.1. EV internalization assay

2.5.1.1. Cell culture

Primary adult human cardiac fibroblasts (HCF; Cell Applications, Inc.) were cultured (passage 2 to 7) in human fibroblast growth medium (FGM; Cell Applications, Inc.) and incubated in a HERAcell® 150 CO_2 incubator (Heraeus®) at 37 ºC in a humidified atmosphere containing 5% CO_2. Cells were routinely observed for assessing confluency and passaged when reaching approximately 80%. For that, cells were detached with 0,25% trypsin/EDTA (Sigma Aldrich, Co.), centrifuged at 300 *x g* for 5 min and seeded with a cell density of 10000 cells/cm^2 in FGM.

2.5.1.2. EV labelling

The equivalent to 10^7 particles/mL of EVs were labelled with the cell membrane binding dye PKH26 (Sigma Aldrich, Co.; $\lambda_{excitation}$=551 nm; $\lambda_{emission}$=567 nm) accordingly to the manufacturer instructions. To remove the excess of dye in solution, labeled EVs were transferred to a spin column (Vivaspin® 6 Centrifugal concentrator (Molecular weight cut off – 100 kDa), Sartorius Stedim Biotech, SA), added 4 mL of cold PBS and centrifuged at 2500 *x g* for 30 min at 4ºC. The solution on the lower compartment of the spin column was discarded, EVs were resuspended in 5 mL of cold PBS and centrifuged again at 2500 *x g* (4ºC) until remaining 100 µL of EVs suspension in the spin column top compartment. Labelled EVs were collected and stored at 4ºC until the next day.

2.5.1.3. Culture of HCF with the labelled EVs

The HCF were seeded (15000 cells/cm^2) on top of a glass coverslip (5mm Ø) and incubated in FGM overnight to adhere. EVs suspension was added to the FGM media to obtain a final EV concentration of 10^7 particles/mL. Cells cultured with FGM without EVs were used as controls.

Cells were fixed at 0 h and 12 h after incubation with EVs with 4% paraformaldehyde in PBS for 12 min, permeabilized with 0,1% Triton X-100 (Sigma Aldrich, Co.) in PBS for 5 min and blocked with 1% BSA in PBS for 30 min at room temperature. Coverslips were then incubated in the dark with Phalloidin CruzFluor™ 488 Conjugate (sc-363791, Santa Cruz Biotechnology, Inc.) 1:1000 for 20 min, rinsed twice with PBS and mounted with Vectashield® with 4',6-diamidino-2-phenylindole (DAPI) mounting medium (Vector Laboratories, Inc.). Images were acquired in a Leica TCS SP5 II laser scanning confocal microscope and adjusted for brightness and contrast using Fiji [75].

2.6. Culture of HCF with PF from patients

The cells were cultured as mentioned in section **2.5.1.1** and then were passed and seeded (15000 cells/cm^2) on top of a glass coverslip (5mm Ø) and incubated in a 1:1 of FGM and Dulbecco's Modified Eagle's Medium (DMEM, Gibco®) supplemented with 1 g/L D-glucose, 1 g/L L-glutamine, 25mM HEPES and 25 mM pyruvate overnight to adhere. Then, the HCF were cultured with a media containing 10% PF in DMEM for 2 days. Cells cultured in DMEM or in DMEM with 10ng/mL TGFß1 were used as controls.

After incubation, cells were fixed with 4% paraformaldehyde in PBS for 12 min, permeabilized with 0,5% Triton X-100 (Sigma Aldrich, Co.) in PBS for 5 min and blocked with 4% FBS in 1% BSA in PBS for 1 hour at room temperature. Coverslips were then incubated with an anti-human α-SMA primary antibody (A5228, Sigma Aldrich, Co.) diluted 1:400 in blocking solution overnight at 4º C. Coverslips were then washed 3 times for 5 min in PBS, incubated with Alexa Fluor® 594 donkey anti-mouse (A21203, Thermo Fisher Scientific) 1:1000 in blocking solution for 1 h and washed again as mentioned before. The preparations were mounted using DAPI mounting medium (Vector Laboratories, Inc.) and observed in a Leica DMI 6000 inverted fluorescence microscope. Brightness and contrast were adjusted using Fiji [75].

2.7. RNA Sequencing (RNA-Seq) analysis

miRNA was extracted from PF of 3 and 4 patients of control and MI cohorts, respectively, as described in section 2.4.1 but without adding the spike-in miRNA. Quality of RNA was assessed using a 2100 BioAnalyzer (Agilent) and libraries were constructed according to Ion Total RNA Seq Kit v2 protocol, in which 2,4 ng RNA was left to hybridize and ligate to a unique barcode for sample identification and tracking. Yield and size distribution of amplified cDNA was assessed in the 2100 BioAnalyzer and, because there was a high presence of adaptor dimers, libraries were ran in a 4% agarose gel and the library band was excised, purified using

illustra GFX PCR DNA and Gel Band Purification Kit (GE Healthcare Europe GmbH) and reanalysed in the 2100 BioAnalyzer. Samples were then processed in the Ion Chef™ System (Thermo Fisher Scientific) and the resulting 550™ chip (Thermo Fisher Scientific) was sequenced on the Ion S5™XL System (Thermo Fisher Scientific) for 2 h and 30 min. The obtained data was processed using the Ion Torrent platform specific pipeline software Torrent Suite v5.8 (smallRNA Plugin) to generate sequence reads, trim adapter sequences, filter and remove poor signal reads, and split the reads according to the barcode. Reads were aligned to mature miRs using the bowtie2 alignment software. Unmapped reads are further aligned to the whole genome to rescue miRbase unaligned reads and count other RNA molecules. RNA sequencing was performed at the GenCore i3S Scientific Platform.

Differential expression analysis between patient cohorts was determined with the Limma-Voom method in the application DEApp [76]. To be considered differently expressed, the normalized counts had to have a fold change (FC) of 1,5 between sample groups and the false discovery rate (FDR) adjusted p-value had to be lower than 0,05. Finally, DNA intelligent Analysis (DIANA) miRPath v.3.0, a web-based microRNA-targeted pathway analysis algorithm [77], was used to identify the Kyoto Encyclopedia of Genes and Genomes (KEGG) pathways that might be altered by the differently expressed miRs. To verify the latter, the database DIANA-Tarbase v8 [78] was used. Heatmaps were generated using the Heatmapper web server [79].

2.8. Statistical Analysis

Data statistical analysis was done using GraphPad® Prism 6 software. Given the low number of samples in each patient group, the data was not considered normally distributed. So, non-parametric tests (Mann-Whitney U test) were used to test all the obtained data. Spearman correlations were also used to assess any correlation between variables. The statistical significance level chosen for all statistical tests was $p<0,05$.

CHAPTER III – RESULTS

3.1. PF concentrates biomarkers of cardiac fibrosis

Peripheral blood and pericardial fluid (PF) were collected from patients with a recent first MI episode (*n*=24, MI group) and compared to patient patients with stable angina (*n*=6, control group (CTRL)), without previous MI or acute coronary syndrome. The two groups were similar in terms of age, sex, age, cardiovascular risk factors and medication at the time of surgery (**Table 3 and 4**). Left ventricle ejection fraction (LVEF) was decreased in the MI group, owning to tissue damage triggered by the blockage of coronary arteries, which contrasts with the control group composed of stable coronary patients.

ST-2 has been proposed as a novel biomarker of cardiac fibrosis [80]. This soluble molecule works as a decoy receptor of IL-33 which prevents fibrosis and cardiomyocyte hypertrophy [80], neutralizing this cardioprotective effect [81]. In order to investigate whether the PF after MI concentrates pro-fibrotic signals, the level of soluble ST2 was quantified in PF and plasma of MI and control patients by ELISA. No apparent changes were detected in the circulating levels of ST-2 in both groups when compared to plasma, ST-2 levels in the PF of both patient cohorts were increased. However, no significant differences were found in PF and plasma ST-2 levels between of MI and stable angina patients (**Figure 4A**). Of note, levels of ST-2 in the PF and plasma of stable angina patients were positively correlated whereas no clear correlation was observed between ST-2 levels in the plasma and PF of MI patients (**Figure 4B)**. Also, no correlation was found between levels of this biomarker and cardiac function (LVEF) across biological fluids and groups (**Supplementary Table 1**).

The degree of inflammation after MI varies along with the different phases of the reparative response. Since our samples were collected at different periods after MI, we hypothesized that, this parameter could be creating variability and masking possible correlations. Hence, we restricted our analysis to samples collected 8-30 days after MI, does discarding the early-phase and chronic phase of the reparative process (**Figure 4C**). In these patients, PF ST-2 levels were negatively correlated with LVEF, whereas circulating ST-2 although showed the same trend but not reaching statistical significance.

3.2. PF from MI patients stimulate myofibroblast differentiation *in vitro*

After observing increased levels of the cardiac fibrosis-associated biomarker ST-2 in the PF, we compared the pro-fibrotic potential of this biological fluid between the two patient cohorts. For that, PF was included as a supplement in *in vitro* culture of human ventricular fibroblasts and the differentiation in myofibroblasts was assessed after 48 hours by immunolabelling of α-SMA (**Figure 5**). A small fraction of fibroblasts cultured in the presence of PF up-regulated the expression of α-SMA and became large and polygonal, when compared to the surrounding cells and cells cultured in basal media (not shown) which were small and elongated (**Figure 5A)**. Quantification of α-SMA-expressing cells demonstrated that the PF collected from MI patients increased the expression of this markers in fibroblasts when

compared to control patients, albeit not reaching statistical significance likely due to the low number of tested samples (**Figure 5B**). These finding support that PF collected from MI patients may stimulate the differentiation of fibroblasts into myofibroblasts, contributing to the pro-fibrotic environment created after MI.

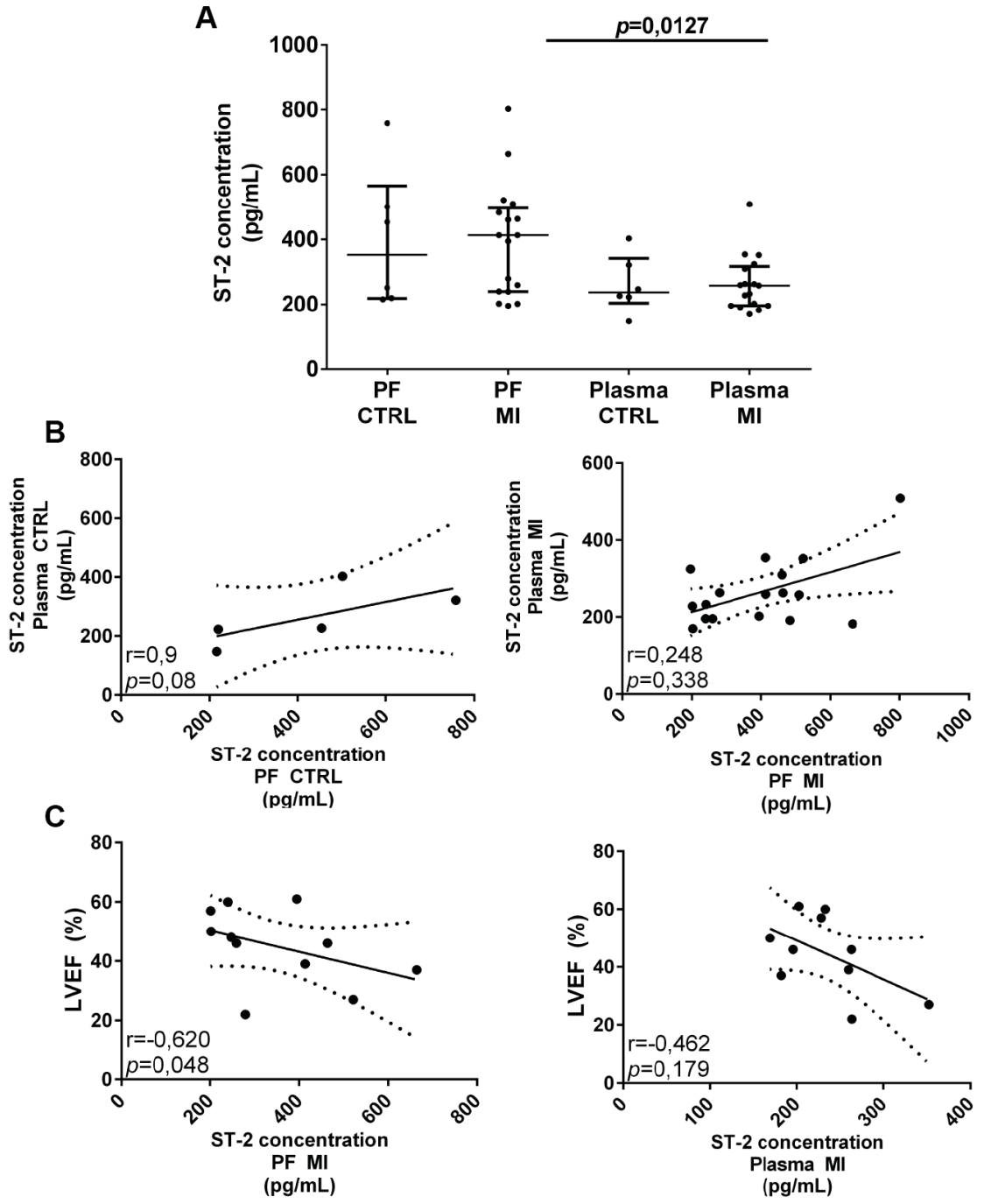

Figure 4: A. ST2 quantification on PF and plasma collected from MI (n=17 in PF and plasma) and stable angina (CTRL) patients (n=6, PF and plasma). Each dot represents a patient measurement and the bar and whiskers represent the median and interquartile range of the results. **B.** Spearman correlation between plasma and PF ST-2 levels of both patient cohorts (n=5, CTRL; n=17, MI). **C.** Spearman correlation between LVEF and ST-2 levels in plasma and PF collected 8-30 days after MI (n=11, plasma and PF) The adjusted line and 95% confidence intervals (dotted lines) are shown in each correlation graph.

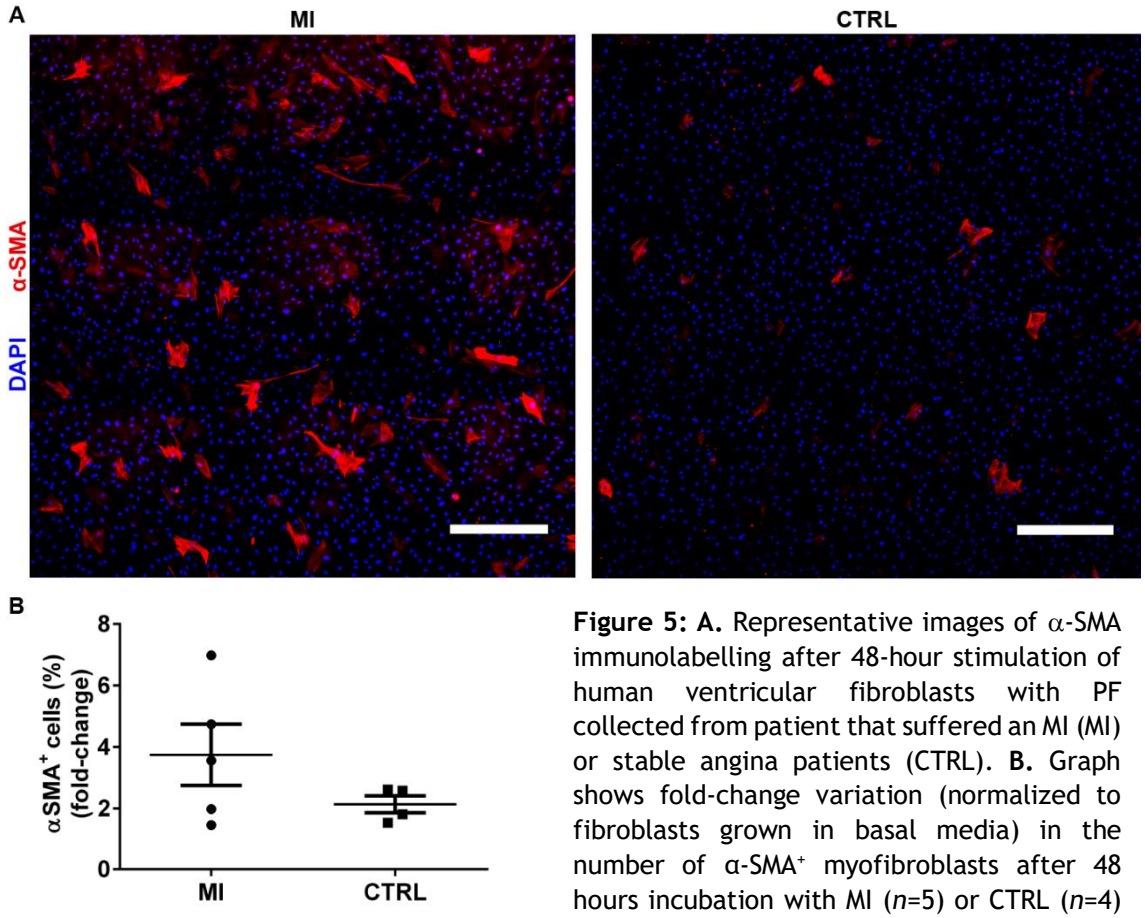

Figure 5: A. Representative images of α-SMA immunolabelling after 48-hour stimulation of human ventricular fibroblasts with PF collected from patient that suffered an MI (MI) or stable angina patients (CTRL). **B.** Graph shows fold-change variation (normalized to fibroblasts grown in basal media) in the number of α-SMA⁺ myofibroblasts after 48 hours incubation with MI (*n*=5) or CTRL (*n*=4) PF (Scale bar, 500 µm). All values are presented as means ± standard error of the mean (SEM).

3.3. Cardiac fibroblast-associated miRs are concentrated in PF compared to plasma

In heart failure, altered levels of miRNA have been detected in the heart-tissue as well as in the plasma, as miRNAs can be released into circulation [82]. Several of these miRNAs have been reported to regulate the formation of cardiac fibrosis and subsequently influence cardiac function [83-85]. Recently, PF microRNA profiling revealed that this body fluid contains several of those small molecules, but no differences were found between disease aetiology groups [41]. Before initiating a high-throughput analysis of the PF miRNA content, we decided to evaluate a selection of previously reported miRNAs in PF and that have been related to cardiac fibrosis. According to Kuosmanen et al. [41], miR-21-5p, miR-29a-3p and miR-29c-3p fulfilled these criteria and were therefore analyzed in PF and plasma from MI and control patients (**Figure 6**).

Regarding miR-21, levels were concentrated in the PF of both patient cohorts, when compared to plasma. In addition, this molecule was more abundant in the PF of MI patients compared to controls (p=0,0206).

MiR-29a and miR29c belong to the miR-29 family and have identical mature sequences but are encoded by different genes and regulated by transcriptional regulators and signalling pathways [86]. In the case of miR-29a, relative expression was increased in PF in both patient groups compared to plasma (p=0,0159, CTRL; p=0,0002, MI). However, no significant

differences were detected on PF or plasma between the two patient cohorts, despite a tendency was observed for higher PF and circulating levels of miR-29a in MI patients, compared to stable angina controls. Similar results were obtained for miR-29c which was concentrated in the PF compared to plasma (p=0,0195, CTRL; p<0,0001, MI) but no differences were observed between patient groups.

Also, all before-mentioned miRs are shown to be highly correlated with each other in PF of MI patients, which is indicative that there is an increase in the release of all tested miRs in this biological fluid, suggesting that some of the collected are biological samples are concentrated in comparison to others.

These findings, in addition to ST2 quantification, support the hypothesis that cardiac fibrosis markers accumulate in the PF in disease situations. Of note, in the case of MI a tendency was obtained for higher concentration of these molecules which may in turn impact on myocardial fibroblast activation.

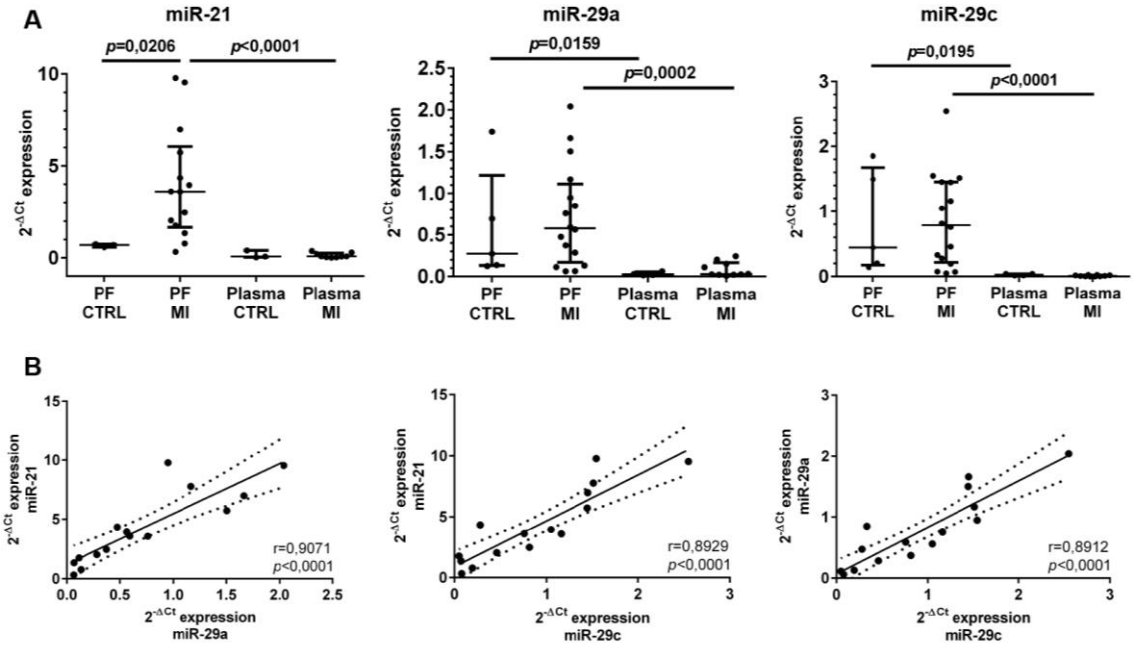

Figure 6: A. Relative expression of miR-21-5p, miR-29a-3p and miR-29c-3p in PF and plasma from MI patients (n=14 in miR-21-5p quantification using PF and n=9 using plasma; n=16 in PF and n=10 in plasma in the quantification of the other miRs) and control patients (n=3 in PF and plasma in the miR-21-5p quantification; n=5 in PF and n=4 in plasma in the quantification of the other miRs). The bar and whiskers represent the median and interquartile range of the results. **B.** Spearman correlation between the measured miRs relative expression in PF of MI patients. The adjusted line and 95% confidence intervals (dotted lines) are shown in each correlation graph.

3.4. Deep-sequencing highlight miRNAs altered in the PF of MI patients

After confirming with a selected panel of miRs that PF concentrates miR signaling from the heart, a high-throughput analysis of the PF miR content in the two patient cohorts was performed (n=4, MI; n=3, CTRL). This analysis allowed the identification of 704 miRs in the PF, with an average of ~110 miRs per sample. The five most abundant microRNAs in PF, regardless

of the disease, were miR-320a, miR-451a, miR-193a-5p, miR-125b-5p, miR-125b-5p, miR-30d-5p.

Given the lack of prior studies using deep sequencing in PF, our results were firstly compared to the only available miR profiling, by Kousmanen and colleagues, of the PF obtained using microarrays for 742 miRs [41]. In brief, from the list of the 50 most abundant miRs in both works, 17 and 46 were present in all PF samples in Kousmanen and our analysis, respectively. A Venn diagram summarizing these results, showed that 9 out of 17 miRs reported by Kousmanen and colleagues, are also present in our list. Of note, the miRs miR-125b-5p, miR-320b, miR340-5p, miR-497-5p, miR-99b-5p and let-7d-3p, which have been reported as specific to the PF when compared to other biological fluids, were all present in our samples, with a coverage of 100% **(Figure 7)**.

Heat map unsupervised clustering of our data failed to discriminate samples according to the pathology, highlighting the variability amongst patients in the same cohort **(Figure 8)**. Nonetheless, we decided to proceed with the analysis in order to detect abnormally expressed miRNA after MI using the limma-voom algorithm [87] with a FC threshold of 1,5 and FDR adjusted p-value of <0,05. Overall, 24 miRs were differentially expressed between MI and CTRL, from which 19 were upregulated in MI patients (**Table 8**).

To further investigate the signaling pathways that were being regulated by altered miRs in the PF of MI patients, DIANA miRPath v.3.0 software was used to obtain experimentally confirmed interactions between miRs and target genes and their involvement in KEGG pathways (**Figure 9**). Of note, since many miRs have not an experimentally validated target, several differently expressed miRs in our analysis showed no indexed interactions and, therefore, could not be included in the KEGG analysis. These miRs are highlighted in **Table 8**.

KEEG pathways analysis revealed that miRs upregulated in PF of MI patients putatively regulate the fatty acid metabolism and ECM-receptor interactions whereas pathways impacted by downregulated miRs are the Hippo signaling pathway and adherens junctions. These findings indicate that the shift in cellular metabolism and ECM remodeling that takes place after MI [88, 89], results in the production of miRs that accumulate in the PF. Further validation of putatively altered miRs after MI and the inclusion of more samples in the analysis which be fundamental to improve our understanding on the signaling pathways regulated by this body fluid.

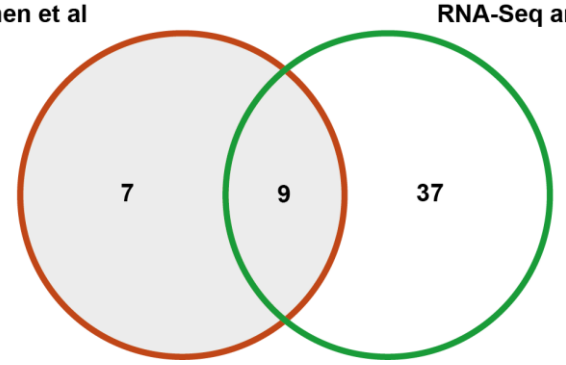

miRNA	Presence
hsa-miR-320a	7 (100%)
hsa-miR-23a-3p	7 (100%)
hsa-miR-423-3p	7 (100%)
hsa-miR-21-5p	7 (100%)
hsa-miR-221-3p	7 (100%)
hsa-miR-23b-3p	7 (100%)
hsa-miR-19b-3p	7 (100%)
hsa-miR-24-3p	7 (100%)
hsa-miR-99a-5p	7 (100%)

Figure 7: Venn diagram comparing the list of most abundant miRs (top 50) detected on all analysed samples of in the present RNA deep-sequencing analysis and the Kuosmanen et al. work. The list of common miRs is detailed in the table on the right.

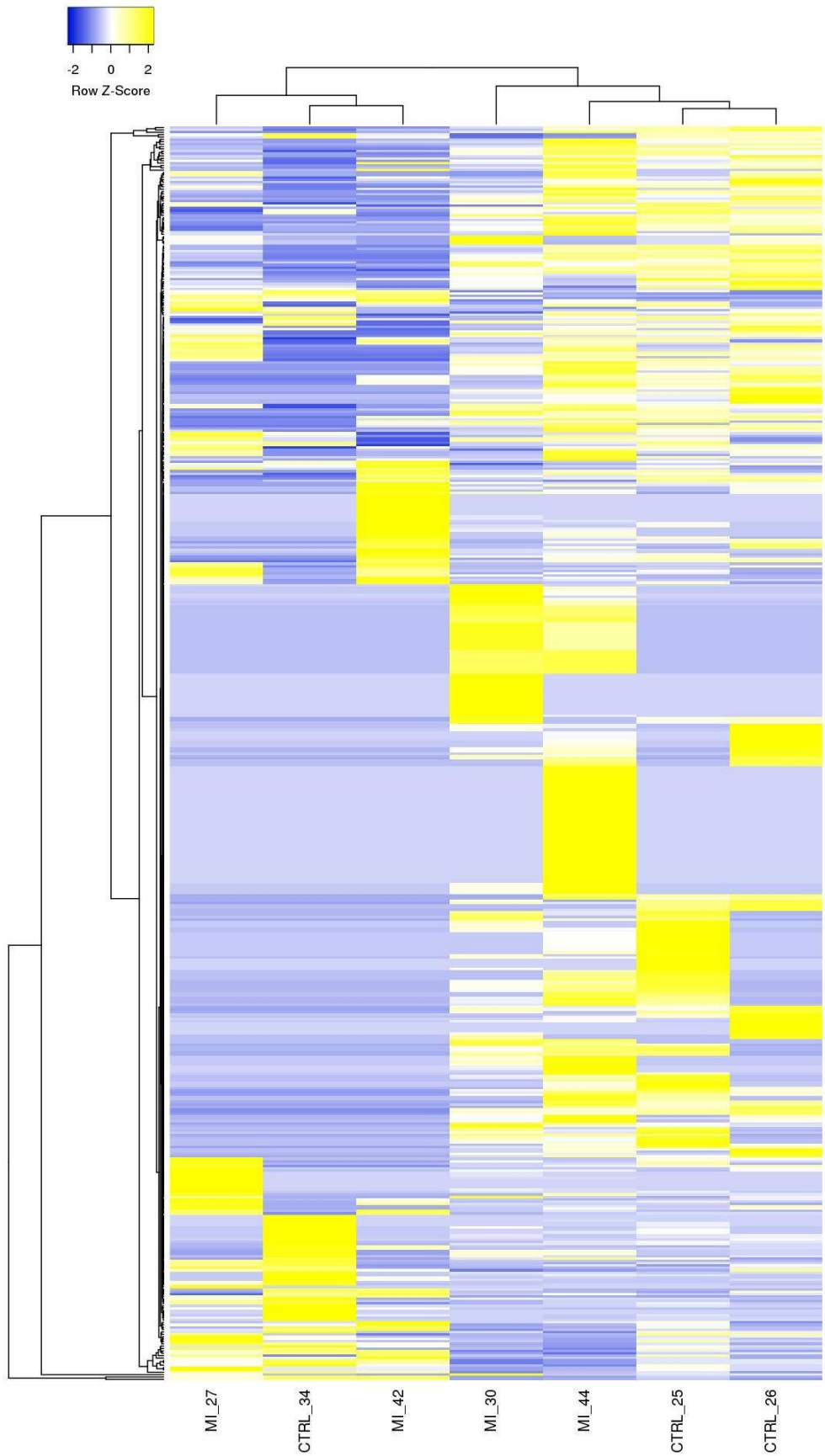

Figure 8: Heat map and unsupervised clustering (Manhattan distance, complete linkage) of the samples (n=3, CTRL; n=4, MI) based on expression of miRs. microRNAs with low expression in blue, miRNAs with high expression in yellow.

.

Table 8: Differently expressed miRs in PF of MI (*n*=4) and stable angina patients (*n*=3) using the limma-voom algorithm.

miR tag	log_2(FC)	p value	FDR p-value
Down-regulated miRNAs in MI			
hsa-miR-320d-2	2,209	0,0026	0,0475
hsa-miR-133a-3p*	2,146	0,0010	0,0215
hsa-miR-320d-1	2,043	0,0008	0,0194
hsa-miR-3960	2,009	0,0015	0,0289
hsa-miR-28-5p	1,996	0,0008	0,0194
Up-regulated miRNAs in MI			
hsa-miR-124-3p	-5,192	0,0011	0,0229
hsa-miR-93-3p	-3,837	0,0002	0,0131
hsa-miR-424-3p	-3,820	0,0003	0,0131
hsa-miR-378d	-3,044	0,0001	0,0122
hsa-miR-550b-2-5p	-3,014	0,0001	0,0122
hsa-miR-550a-3p	-3,014	0,0001	0,0122
hsa-miR-1292-5p*	-3,009	0,0002	0,0131
hsa-let-7e-3p	-3,003	0,0001	0,0122
hsa-miR-6747-3p*	-2,993	0,0004	0,0131
hsa-miR-6087*	-2,988	0,0004	0,0131
hsa-miR-576-3p	-2,982	0,0004	0,0131
hsa-miR-92b-5p	-2,978	0,0002	0,0131
hsa-miR-30c-1-3p	-2,938	0,0005	0,0148
hsa-miR-203a*	-2,927	0,0004	0,0131
hsa-miR-203b-5p*	-2,927	0,0004	0,0131
hsa-miR-33a-5p	-2,917	0,0005	0,0148
hsa-miR-204-3p	-2,916	0,0001	0,0122
hsa-miR-331-3p	-2,894	0,0007	0,0178
hsa-miR-1273g-3p	-2,893	0,0012	0,0229

*miRs that had no interactions detected in DIANA-Tarbase v8

3.5. Pericardial fluid contains EVs that are capable to internalize human ventricular fibroblasts

Extracellular vesicles (EVs) are known to carry and deliver miRs and other bioactive molecules to cells. We hypothesized that at least part of the miRNA-related bioactive properties of the PF could be mediated by EVs. hence, EVs were isolated from PF and plasma from both patient groups by ultracentrifugation and characterized to further study the biological impact of those vesicles. Electronic microscopy further confirmed the presence and unveiled the morphology of EVs (**Figure 10**). Cup shaped vesicles of different sizes were observed by negative staining in all samples from both patient groups, confirming that EVs were successfully isolated. Also, it was observed that mainly small EVs could be seen in most of the analyzed samples. EVs size distribution and concentration was further assessed using NTA (**Figure 10 and Table 9**). From both biological sources, the isolated EVs had a size ranging 10 to 500 nm in diameter with a prevalence of EVs with sizes of approximately 100 nm. Regarding EV concentration, there is a significant increase in particles in PF compared to plasma.

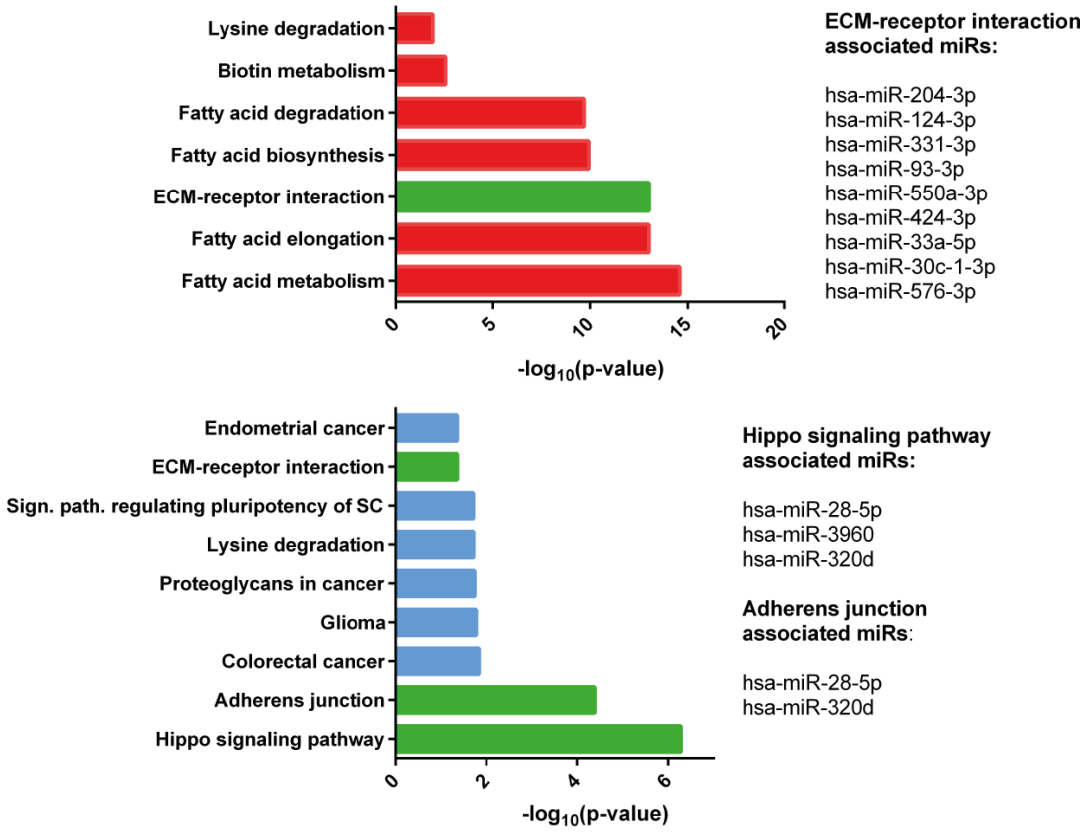

Figure 9: KEGG pathways of upregulated (upper graph) and downregulated (lower graph) miRs in MI patients when comparing to the control (stable angina). In green, highlighted the KEEG pathways relevant for the present study and the respective miRs involved (right).

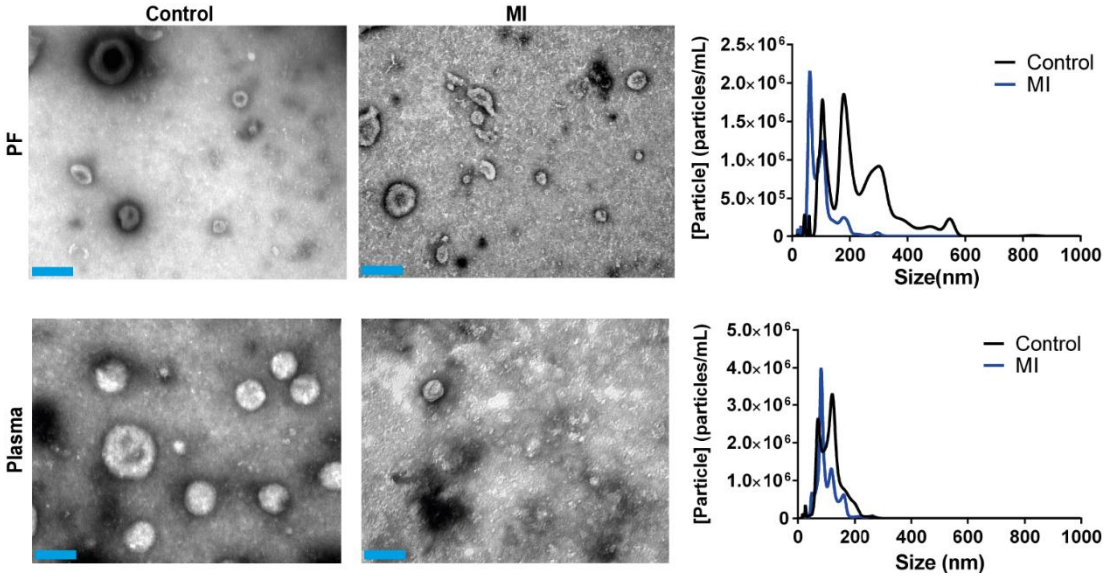

Figure 10: Representative TEM images and NTA analysis of the EVs isolated from PF (n=3 in control patients and n=6 in MI patients) and plasma (n=2 in control patients and n=7 in MI patients) from both patient groups (scale bar=200 nm).

Table 9: Parameters measured by NTA of EVs isolated from plasma and PF from both patient groups. Results are the mean of all the measured samples (PF: Control n=3 and MI n=6; Plasma: Control n=2 and MI n=7)

Samples		Particle concentration (particles/mL)	Mode(nm)
PF	Control	$5,41\pm0,66x10^{10}$	140,3±13,1
	MI	$4,04\pm0,67x10^{10}$	124,6±32,6
Plasma	Control	$3,01\pm0,30x10^{10}$	98,8±11,6
	MI	$2,83\pm0,23x10^{10}$	92,8±12,0

To further characterize the isolated EVs, the presence of EV markers was investigated using WB (**Figure 11**). The latter are molecules involved in EV biogenesis, in particular, the tetraspanins CD63 and CD81, the ESCRT protein Alix and the cytosolic proteins Hsp70 and Flotillin-1. Also, Cytochrome-C, a cell organelle marker, was used to analyze if cell debris from the biological fluid could be contaminating the EVs preparation.

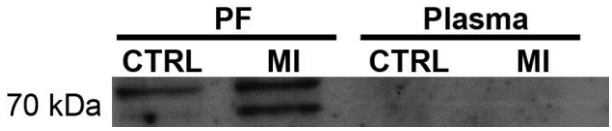

Figure 11: Analysis of Hsp70, a classical EVs marker, in EVs isolated from PF and plasma obtained from both patient groups by WB.

Hsp70 was identified in EVs collected from PF samples of both patient groups but not in plasma. In addition, cytochrome-c was not detected in EVs obtained from all samples, indicating that cellular contaminants are not at a detectable range in EVs. Regarding the WB of other markers, no band was clearly evident, likely because WB requires a substantial amount of biological material, which can be very demanding in the context of EV extracts isolated from surgical samples.

Having confirmed the presence and partially characterized the PF and plasma EVs we tested whether these vesicles could have any biological activity. To assess the latter, a co-culture of human ventricular fibroblasts with PKH-stained EVs was performed and the cells were fixed at 0h and 12h. As expected, at the first timepoint no internalization of EVs was observed whereas after 12h of co-culture, red labelling was evident inside cells cultured with stained EVs (confirmed with orthogonal view), suggesting EVs were internalized by cells. Although in the timeframe of the present MSc dissertation no further *in vitro* studies could be performed, this experiment supports further investment on understanding the biological impact of these EVs on cells.

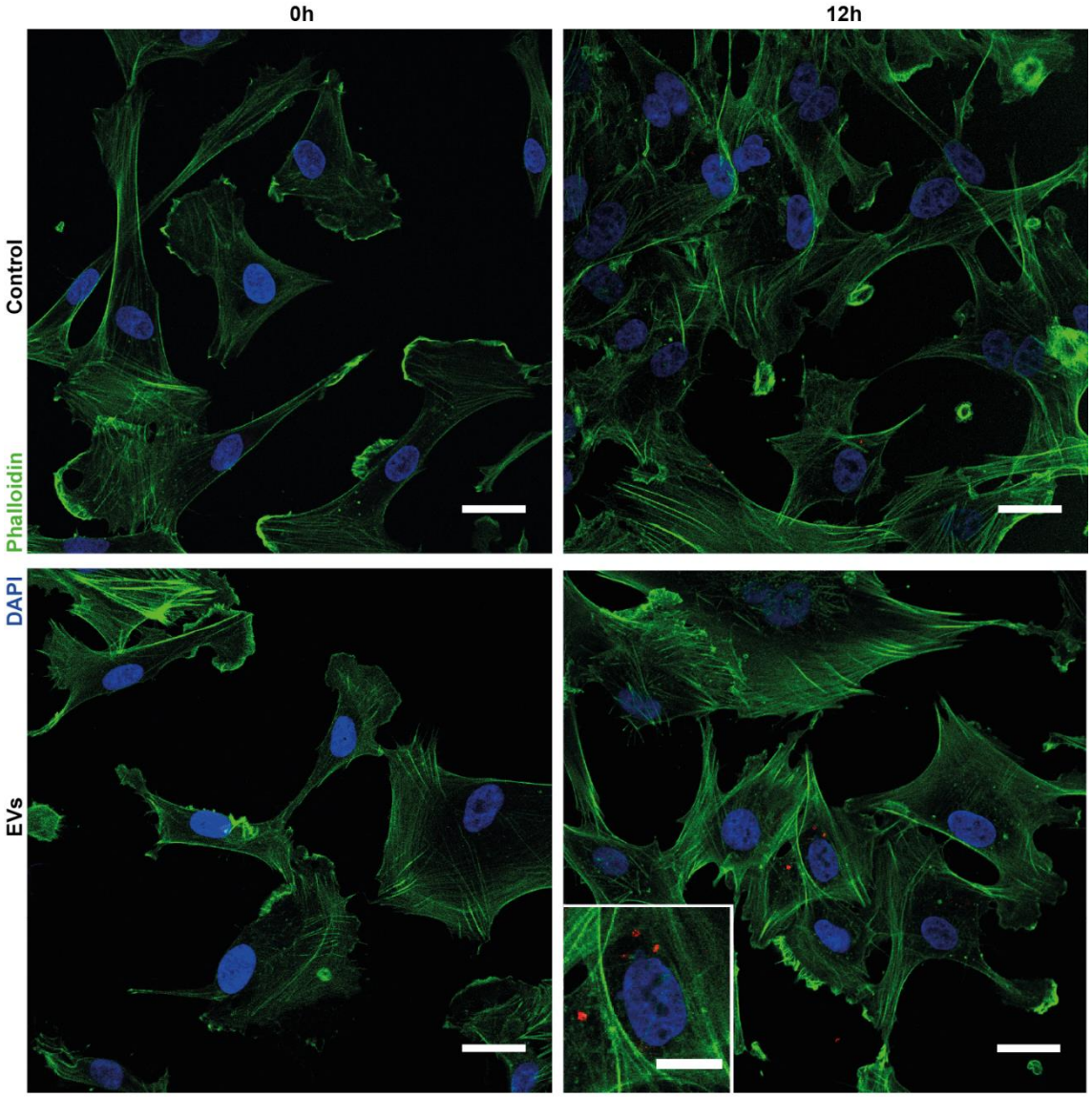

Figure 12: Representative images of human ventricular fibroblasts co-cultured with PKH26-stained EVs (red) and respective controls (cells cultured without EVs). Representative data of two independent experiments (scale bar=30 µm and 15 µm in the inset).

CHAPTER IV – DISCUSSION

IHD is the leading cause of death worldwide constituting a major socio-economic burden. Amongst ischemic heart diseases, MI is the major cause of morbidity and mortality and therefore development of novel therapeutic solutions for this disease is of great biomedical relevance. PF has been recently regarded as a potential source of molecular targets that can be modulated to promote regeneration or more efficient heart repair since it concentrates several factors produced by cardiac cells. Hence, molecular targets present in the PF may be of therapeutic relevance, namely, to attenuate cardiac remodeling.

The aim of this study was to evaluate the impact of PF on the activation of cardiac fibrosis and identify altered molecules in PF of MI patients with potential to integrate anti-fibrotic therapies for MI. For that, PF and plasma were collected from patients that suffered recent MI and patient with stable angina, i.e. stable coronary syndrome but without detectable myocardial death. We showed that the PF after MI i) accumulates fibrotic markers, namely miR-21, ii) stimulates the differentiation of cardiac fibroblast in myofibroblasts, iii) contains EVs capable of internalizing on cardiac fibroblasts and iv) displays a different miR profiling, compared to the PF of stable angina patients, that may regulate cardiac remodeling.

To assess the presence of cardiac fibrosis markers, the level of soluble ST2 was quantified in PF and plasma of MI and control patients. Several evidence indicate that cardiomyocytes, fibroblasts and endothelial cells contribute to ST-2 production [90-92]. Our data is in line with these observations since ST2 levels in the PF were in average ~1,5-fold higher compared to plasma, suggesting that is being produced mainly by heart cells. Indeed, the IL-33/ST2 system has been suggested as a novel cardioprotective axis mediated by fibroblast–cardiomyocyte interplay. In response to biomechanical strain, these cells produce mature IL-33, which reduces hypertrophic response of cardiomyocytes *in vitro*, a process that can be reverted by ST-2, working as a IL-33 decoy receptor [93]. One can then speculate that the higher concentration of ST-2 in the PF may worsen ventricular remodelling after MI. This is of particular importance owing to a great debate among clinicians whether or not the pericardium should be closed after cardiac surgery [94].

A positive correlation was observed between soluble ST2 levels in PF and plasma in control patients and, at a less extend, in MI patients. Interestingly, although no correlation was found with left ventricular ejection fraction across groups and biological fluids, if the analysis was restricted to patients that suffered an MI in the past 8-30 days, a clear correlation was observed, in particular in the PF. The correlation of ST-2 circulating levels and LVEF was already reported in prior studies [90, 95] however the number of samples were higher than the available in the present study. Nevertheless, despite the restricted amount of samples in the present study, a strong correlation was attained between PF ST-2 levels and cardiac function.

A bi-model distribution can be observed regarding ST-2 measurements in the PF of MI, and at less extent, stable angina patients, increasing variability. Regrettably, the number of samples in the present study is limiting for correlating ST-2 levels with cardiovascular risk factors in each group. Notwithstanding, some measurements were several fold higher than average values of the remaining group. In the case of PF from control patients, the sample was obtained from the only female patient that suffered from unstable angina 8 months before

surgery that evolved to stable angina, this can be one explanation for increased ST2 levels. The BMI of the same patient was in the borderline obese (BMI=30,59 kg m^{-2}, when BMI>30 kg m^{-2} is considered obesity) and severe obesity has been shown to increase soluble ST2 levels [96]. In these patients with BMI>40 kg m^{-2} were compared to patients with BMI<30 kg m^{-2}, meaning that the abnormal value obtained was not related with this parameter. Another explanation is that the patient hypertensive, which can elevate soluble ST2 levels [97]. In the case of PF and plasma from MI patients, the higher value in both groups are from a patient that was subjected to surgery in critical state after a ST-elevation myocardial infarction (STEMI), in which an intra-aortic balloon pump had to be used to stabilize the patient before the medical procedure. Finally, regarding the elevated levels of soluble ST2 in plasma from control patients, there was a measurement in plasma obtained on a patient that suffered from chronic obstructive pulmonary disorder and peripheral arterial disease at the time of surgery which can explain the increase circulating ST2 levels as reported in several studies [98, 99].

Other fibrosis-associated molecules, namely miR-21-5p, miR-29a-3p and miR-29c-3p, were also quantified in the PF and plasma of the two patient cohorts. These miRs were shown to have different interactions after MI and cardiac remodeling. MiR-21-5p was shown to be upregulated in case of MI and influence posterior cardiac fibrosis [100, 101] by increasing fibroblast MMP-2 expression, promoting TGF-β1-induced fibroblast transformation to myofibroblasts and its inhibition has been reported to decrease cardiac fibrosis [46, 101, 102]. Herein, miR-21-5p was shown to be concentrated in the PF of MI patients compared to controls.

In the other hand, miR-29a-3p and miR-29c-3p are part of the miR-29 family [86]. This family has been shown to impact cardiac fibrosis after MI since TGF-β expression downregulates miR-29 expression by cardiac fibroblasts, resulting in an upregulation of several ECM proteins [85]. The relation between miR-29 and ECM production was further proved by knocking down miR-29 *in vivo*, resulting in upregulation of collagen expression [85]. The quantification of these miRs shown that PF has higher concentration compared to plasma and no differences were observed regarding disease groups.

The pro-fibrotic environment created following MI in the PF, herein shown by increased levels of ST2 and miR-21-5p, was further supported by evidence that PF collected from patients with MI increased activation of human cardiac fibroblasts to myofibroblasts. However, further studies are required to understand the underlying mechanisms.

Given the lack of studies regarding PF, deep-sequencing was performed to obtain a portrait of miRs present in the PF. Of interest, 4 out of the 5 most abundant miRs in our analysis have been reported to be detected in coronary sinus samples, from which miR-125-5p, miR-451a and miR-320 were shown to be up-regulated in heart failure.

Twenty-four miRs were shown to be differentially expressed in the two patient cohorts. Albeit these results require further validation in more samples, these miRs may constitute potential targets for therapy and/or biomarker research. These results contrast with the report from Kousmanen and colleagues that, by using microarrays that measured 742, were not able to discriminate samples according to the clinical features of the patients. One possible explanation for the contradictory results relies on the different methodology used. Herein, we

used deep-sequencing which allowed the identification of 704 miRs with an average of ~110 miRs per sample. The other approach identified an average of 256 microRNAs per sample but used a targeted approached (microarrays) that fails to detect differences in miRs outside the analyzed panel.

Regarding signaling pathways putatively impacted by the differently expressed genes, upregulated miRs in MI patients are involved in the regulation of fatty acid metabolism and ECM-receptor interaction. Commonly, the upregulation of miRs translates to a decrease in the activity of the impacted pathways. Interestingly, ischemic hearts have been shown to have impaired fatty acid transport and oxidation and upregulated expression of glucose channels, indicative of a metabolic shift to a preferentially glycolytic state [88]. To complement the latter, patients that suffer from an abnormal glucose metabolism have been shown to have higher impairment of left ventricle function after MI [103]. Regarding the impact in ECM-receptor interaction, it is known that after ischemia an inflammatory phase is initiated, which activates latent MMPs that remodel the cardiac ECM causing the production of ECM fragments that will function as potent inflammatory mediators [89]. This process produces a provisional matrix that will further impact the repair of the infarcted heart, which can explain the downregulation of several genes included in the ECM-receptor interaction pathway.

On the other hand, downregulated miRs were shown to influence Hippo signaling pathway and the adherens junctions. These pathways are tightly related because Hippo signaling mediates the control of cell proliferation by contact inhibition, in which the adherens junctions function as mediators [104]. Also, the Hippo signaling pathway has been shown to increase caspase activation, cardiomyocyte apoptosis and to progressively deteriorate of cardiac function, perhaps as a result of elevated cardiac wall stress that leads to increased myocardial oxygen consumption and apoptosis [105]. In contrast, Hippo pathway can activate other signalling pathways that restores heart function and stimulate cardiomyocyte re-enter in the cell cycle, thus inducing cardiac proliferation after MI [106].

Cell-free miRNAs can circulate incorporated into extracellular vesicles (EVs) which may work as cell delivery systems. EV were isolated by ultracentifugation from plasma and PF of both patient groups and no differences were detected concerning size but there was a significant increase of particle concentration in PF However, most of the EV markers tested in WB could not be detected in isolated EVs from both biological fluids, which may relate to the low concentration of protein present in the EV extracts and contamination by albumin and lipoprotein that interferes with the classical EV marker detection. Hence, further WB optimization is required to achieve a complete EVs characterization.

Overall, these findings show for the first time that the macro-niche established between the heart and PF is crucial for the activation of fibrosis following MI and identifies miRs putatively relevant for this process.

CHAPTER V – CONCLUDING REMARKS

5.1. Concluding remarks

The main goal of the herein work was to assess whether the PF regulates the formation of cardiac fibrosis in the context of MI and identify novel targets with potential to integrate anti-fibrotic therapies.

By pairwise comparison of PF and plasma of two patient cohorts, i.e. patient with MI and patients with stable angina, we were able to show that several pro-fibrotic factors were present in higher concentration in PF of MI patients compared to plasma, promoting cardiac fibroblast activation *in vitro*. In addition, deep-sequencing of PF revealed a diversity of processes putatively affected by PF and identified miRs differentially expressed after MI which, following subsequent validation, may constitute valuable targets for anti-fibrotic therapies.

Overall these findings advocate PF as a valuable source to discover new therapeutic targets for the treatment of myocardial infarction.

5.2. Future perspectives/work

The results obtained during the herein MSc dissertation, although promising, still require further investment:

i) Collection of surgical samples needs to continue, in particular for the control group, in order to increase robustness of our findings and to investigate if fibrotic markers and the identified miRs correlate with other variables, namely cardiovascular risk factor and demographic parameters.

ii) Western Blot conditions require optimization in order to detect classical EV markers, important for EVs characterization and to analyze whether vesicles isolated from plasma and PF from both patient groups are similar.

iii) The effect of EVs, from the different biological fluids and patient cohorts, in the activation of cardiac fibroblasts should also be addressed to answer if EVs in fact contribute to the pro-fibrotic environment created upon MI.

iv) The list of differentially expressed miRs obtained from the RNA-Seq requires further validation by qPCR, including a higher number of patients. Also, plasma samples should also be included in the validation.

In a longer run, to further validate the potential of the identified miRs to integrate anti-fibrotic therapies for MI we would also have to: i) explore *in vitro* the pro-/anti-fibrotic effect of the selected miRNA; and ii) test a miRNA-targeted therapy on a murine model of MI by evaluating altered function and molecular/cellular processes.

CHAPTER V – REFERENCES

1. Wong, N.D., *Epidemiological studies of CHD and the evolution of preventive cardiology*. Nature Reviews Cardiology, 2014. **11**: p. 276.
2. Moran, A.E., et al., *Assessing the Global Burden of Ischemic Heart Disease: Part 1: Methods for a Systematic Review of the Global Epidemiology of Ischemic Heart Disease in 1990 and 2010*. Global heart, 2012. **7**(4): p. 315-329.
3. Thygesen, K., et al., *Universal definition of myocardial infarction*. Circulation, 2007. **116**(22): p. 2634-53.
4. WHO. *The top 10 causes of death*. 2017; Available from: http://www.who.int/mediacentre/factsheets/fs310/en/.
5. Finegold, J.A., P. Asaria, and D.P. Francis, *Mortality from ischaemic heart disease by country, region, and age: Statistics from World Health Organisation and United Nations()*. International Journal of Cardiology, 2013. **168**(2): p. 934-945.
6. Blom, J.N. and Q. Feng, *Cardiac repair by epicardial EMT: Current targets and a potential role for the primary cilium*. Pharmacol Ther, 2018.
7. Thygesen, K., et al., *Third universal definition of myocardial infarction*. European Heart Journal, 2012. **33**(20): p. 2551-2567.
8. DeWood , M.A., et al., *Prevalence of Total Coronary Occlusion during the Early Hours of Transmural Myocardial Infarction*. New England Journal of Medicine, 1980. **303**(16): p. 897-902.
9. Frangogiannis, N.G., *Pathophysiology of Myocardial Infarction*. Compr Physiol, 2015. **5**(4): p. 1841-75.
10. Sanchis-Gomar, F., et al., *Epidemiology of coronary heart disease and acute coronary syndrome*. Ann Transl Med, 2016. **4**(13).
11. Association, A.H. *CARDIOVASCULAR DISEASE: A COSTLY BURDEN FOR AMERICA PROJECTIONS THROUGH 2035*. 2017; Available from: http://www.heart.org/idc/groups/heart-public/@wcm/@adv/documents/downloadable/ucm_491543.pdf.
12. Wilkins E, W.L., Wickramasinghe K, Bhatnagar P, Leal J, Luengo-Fernandez R, Burns R, Rayner M, Townsend N, *European Cardiovascular Disease Statistics 2017*. 2017: European Heart Network.
13. Frangogiannis, N.G., *The mechanistic basis of infarct healing*. Antioxid Redox Signal, 2006. **8**(11-12): p. 1907-39.
14. Saïd-Sadier, N. and D.M. Ojcius, *Alarmins, Inflammasomes and Immunity*. Biomedical journal, 2012. **35**(6): p. 437-449.
15. Richard, Seidu A., et al., *Pivotal neuroinflammatory and therapeutic role of high mobility group box 1 in ischemic stroke*. Bioscience Reports, 2017. **37**(6): p. BSR20171104.
16. Shinde, A.V. and N.G. Frangogiannis, *Fibroblasts in myocardial infarction: a role in inflammation and repair*. Journal of molecular and cellular cardiology, 2014. **0**: p. 74-82.

17. Frangogiannis, N.G., *Matricellular proteins in cardiac adaptation and disease*. Physiol Rev, 2012. **92**(2): p. 635-88.
18. Hinz, B., et al., *Alpha-Smooth Muscle Actin Expression Upregulates Fibroblast Contractile Activity*. Molecular Biology of the Cell, 2001. **12**(9): p. 2730-2741.
19. Cohn, J.N., R. Ferrari, and N. Sharpe, *Cardiac remodeling--concepts and clinical implications: a consensus paper from an international forum on cardiac remodeling. Behalf of an International Forum on Cardiac Remodeling*. J Am Coll Cardiol, 2000. **35**(3): p. 569-82.
20. Nielsen, E.E., et al., *Beta-blockers for non-acute treatment after myocardial infarction*. 2017.
21. Ibanez, B., et al., *2017 ESC Guidelines for the management of acute myocardial infarction in patients presenting with ST-segment elevationThe Task Force for the management of acute myocardial infarction in patients presenting with ST-segment elevation of the European Society of Cardiology (ESC)*. European Heart Journal, 2018. **39**(2): p. 119-177.
22. Porrello, E.R., et al., *Transient regenerative potential of the neonatal mouse heart*. Science, 2011. **331**(6020): p. 1078-80.
23. Andersen, D.C., et al., *Do Neonatal Mouse Hearts Regenerate following Heart Apex Resection?* Stem Cell Reports, 2014. **2**(4): p. 406-13.
24. Rodriguez, E.R. and C.D. Tan, *Structure and Anatomy of the Human Pericardium*. Progress in Cardiovascular Diseases, 2017. **59**(4): p. 327-340.
25. Vogiatzidis, K., et al., *Physiology of pericardial fluid production and drainage*. Front Physiol, 2015. **6**: p. 62.
26. Michael Francis Oliver, M.L.E., Stanley W. Jacob. *Human cardiovascular system*. 2017 [cited 2018 22 January]; Available from: https://www.britannica.com/science/human-cardiovascular-system.
27. Parmar, Y.J., et al., *Congenital Abnormalities of the Pericardium*. Cardiol Clin, 2017. **35**(4): p. 601-614.
28. Gibson, A.T. and M.B. Segal, *A study of the composition of pericardial fluid, with special reference to the probable mechanism of fluid formation*. J Physiol, 1978. **277**: p. 367-77.
29. Ben-Horin, S., et al., *The composition of normal pericardial fluid and its implications for diagnosing pericardial effusions*. Am J Med, 2005. **118**(6): p. 636-40.
30. Fujita, M., et al., *Pericardial fluid as a new material for clinical heart research*. Int J Cardiol, 2001. **77**(2-3): p. 113-8.
31. Iwakura, A., et al., *Pericardial fluid from patients with unstable angina induces vascular endothelial cell apoptosis*. J Am Coll Cardiol, 2000. **35**(7): p. 1785-90.
32. Foglio, E., et al., *Exosomal clusterin, identified in the pericardial fluid, improves myocardial performance following MI through epicardial activation, enhanced arteriogenesis and reduced apoptosis*. Int J Cardiol, 2015. **197**: p. 333-47.

33. Momen-Heravi, F., S.J. Getting, and S.A. Moschos, *Extracellular vesicles and their nucleic acids for biomarker discovery*. Pharmacol Ther, 2018.
34. Samanta, S., et al., *Exosomes: new molecular targets of diseases*. Acta Pharmacol Sin, 2017.
35. Akers, J.C., et al., *Biogenesis of extracellular vesicles (EV): exosomes, microvesicles, retrovirus-like vesicles, and apoptotic bodies*. Journal of neuro-oncology, 2013. **113**(1): p. 1-11.
36. Chen, Y., G. Li, and M.-L. Liu, *Microvesicles as Emerging Biomarkers and Therapeutic Targets in Cardiometabolic Diseases*. Genomics, Proteomics & Bioinformatics, 2018. **16**(1): p. 50-62.
37. Caruso, S. and I.K.H. Poon, *Apoptotic Cell-Derived Extracellular Vesicles: More Than Just Debris*. Frontiers in Immunology, 2018. **9**(1486).
38. Sluijter, J.P.G., et al., *Microvesicles and exosomes for intracardiac communication*. Cardiovascular Research, 2014. **102**(2): p. 302-311.
39. Ribeiro-Rodrigues, T.M., et al., *Exosomes secreted by cardiomyocytes subjected to ischaemia promote cardiac angiogenesis*. Cardiovascular Research, 2017. **113**(11): p. 1338-1350.
40. Dougherty, J.A., et al., *Potential Role of Exosomes in Mending a Broken Heart: Nanoshuttles Propelling Future Clinical Therapeutics Forward*. Stem Cells International, 2017. **2017**: p. 5785436.
41. Kuosmanen, S.M., et al., *MicroRNA profiling of pericardial fluid samples from patients with heart failure*. PLoS One, 2015. **10**(3): p. e0119646.
42. Graves, P. and Y. Zeng, *Biogenesis of Mammalian MicroRNAs: A Global View*. Genomics, Proteomics & Bioinformatics, 2012. **10**(5): p. 239-245.
43. Yi, R., et al., *Exportin-5 mediates the nuclear export of pre-microRNAs and short hairpin RNAs*. Genes & Development, 2003. **17**(24): p. 3011-3016.
44. Fischer, S.E., *RNA Interference and MicroRNA-Mediated Silencing*. Curr Protoc Mol Biol, 2015. **112**: p. 26.1.1-5.
45. Cipolla, G.A., *A non-canonical landscape of the microRNA system*. Front Genet, 2014. **5**.
46. Fiedler, J. and T. Thum, *MicroRNAs in myocardial infarction*. Arterioscler Thromb Vasc Biol, 2013. **33**(2): p. 201-5.
47. Ikemoto, M., et al., *Development of enzyme-linked immunosorbent assay for acidic fibroblast growth factor and its clinical application*. Clin Chim Acta, 1999. **283**(1-2): p. 171-82.
48. Fujita, M., et al., *Marked elevation of vascular endothelial growth factor and basic fibroblast growth factor in pericardial fluid of patients with angina pectoris*. Angiogenesis, 1998. **2**(1): p. 105-8.
49. Fujita, M., et al., *Elevated basic fibroblast growth factor in pericardial fluid of patients with unstable angina*. Circulation, 1996. **94**(4): p. 610-3.

50. Kubota, T., et al., *Concentrations of hepatocyte growth factor, basic fibroblast growth factor, and vascular endothelial growth factor in pericardial fluid and plasma*. Jpn Heart J, 2004. **45**(6): p. 989-98.
51. Yoneda, T., et al., *Pericardial fluid from patients with ischemic heart disease accelerates the growth of human vascular smooth muscle cells*. Jpn Circ J, 2000. **64**(7): p. 495-8.
52. Ege, T., et al., *Effect of pericardial fluid pro-inflammatory cytokines on hemodynamic parameters*. Cytokine, 2003. **23**(1-2): p. 47-51.
53. Kameda, K., et al., *Increased pericardial fluid level of matrix metalloproteinase-9 activity in patients with acute myocardial infarction: possible role in the development of cardiac rupture*. Circ J, 2006. **70**(6): p. 673-8.
54. Miyamoto, S., et al., *Elevation of matrix metalloproteinase-2 level in pericardial fluid is closely associated with left ventricular remodeling*. Am J Cardiol, 2002. **89**(1): p. 102-5.
55. Abe, N., et al., *Increased Level of Pericardial Insulin-Like Growth Factor-1 in Patients With Left Ventricular Dysfunction and Advanced Heart Failure*. Journal of the American College of Cardiology, 2006. **48**(7): p. 1387-1395.
56. Ren, J., W.K. Samson, and J.R. Sowers, *Insulin-like growth factor I as a cardiac hormone: physiological and pathophysiological implications in heart disease*. J Mol Cell Cardiol, 1999. **31**(11): p. 2049-61.
57. Klemola, R., et al., *Plasma and pericardial fluid natriuretic peptide levels in postinfarction ventricular dysfunction*. Eur J Heart Fail, 2001. **3**(1): p. 21-6.
58. Moltrasio, M., et al., *Brain natriuretic peptide in acute myocardial infarction: a marker of cardio-renal interaction*. J Cardiovasc Med (Hagerstown), 2016. **17**(11): p. 803-9.
59. Ozawa, T., et al., *Effects of human atrial natriuretic peptide on myocardial performance and energetics in heart failure due to previous myocardial infarction*. J Cardiol, 2015. **66**(3): p. 232-8.
60. Corda, S., et al., *Trophic effect of human pericardial fluid on adult cardiac myocytes. Differential role of fibroblast growth factor-2 and factors related to ventricular hypertrophy*. Circ Res, 1997. **81**(5): p. 679-87.
61. Itoh, N. and H. Ohta, *Pathophysiological roles of FGF signaling in the heart*. Frontiers in Physiology, 2013. **4**: p. 247.
62. Iwakura, A., et al., *Pericardial fluid from patients with ischemic heart disease induces myocardial cell apoptotis via an oxidant stress-sensitive p38 mitogen-activated protein kinase pathway*. J Mol Cell Cardiol, 2001. **33**(3): p. 419-30.
63. Cheng, Y. and C. Zhang, *MicroRNA-21 in Cardiovascular Disease*. Journal of cardiovascular translational research, 2010. **3**(3): p. 251-255.
64. Wang, X., et al., *Loss of the miR-144/451 cluster impairs ischaemic preconditioning-mediated cardioprotection by targeting Rac-1*. Cardiovascular Research, 2012. **94**(2): p. 379-390.

65. Huang, S., et al., *Circulating MicroRNAs and the occurrence of acute myocardial infarction in Chinese populations*. Circ Cardiovasc Genet, 2014. **7**(2): p. 189-98.
66. Bao, M.-H., et al., *Let-7 in Cardiovascular Diseases, Heart Development and Cardiovascular Differentiation from Stem Cells*. International Journal of Molecular Sciences, 2013. **14**(11): p. 23086-23102.
67. Vegter, E.L., et al., *Low circulating microRNA levels in heart failure patients are associated with atherosclerotic disease and cardiovascular-related rehospitalizations*. Clinical Research in Cardiology, 2017. **106**(8): p. 598-609.
68. Vegter, E.L., et al., *MicroRNAs in heart failure: from biomarker to target for therapy*. European Journal of Heart Failure, 2016. **18**(5): p. 457-468.
69. Miyamoto, S., et al., *Expression Patterns of miRNA-423-5p in the Serum and Pericardial Fluid in Patients Undergoing Cardiac Surgery*. PLoS One, 2015. **10**(11): p. e0142904.
70. Beltrami, C., et al., *Human Pericardial Fluid Contains Exosomes Enriched with Cardiovascular-Expressed MicroRNAs and Promotes Therapeutic Angiogenesis*. Mol Ther, 2017. **25**(3): p. 679-693.
71. Watanabe, M., et al., *The roles of natriuretic peptides in pericardial fluid in patients with heart failure*. Clin Cardiol, 2009. **32**(3): p. 159-63.
72. Limana, F., et al., *Myocardial infarction induces embryonic reprogramming of epicardial c-kit(+) cells: role of the pericardial fluid*. J Mol Cell Cardiol, 2010. **48**(4): p. 609-18.
73. Fernández, A.L., et al., *Biochemical markers of myocardial injury in the pericardial fluid of patients undergoing heart surgery☆*. Interactive CardioVascular and Thoracic Surgery, 2008. **7**(3): p. 373-377.
74. Kränkel, N., S. Blankenberg, and T. Zeller, *Early detection of myocardial infarction—microRNAs right at the time?* Annals of Translational Medicine, 2016. **4**(24): p. 502.
75. Schindelin, J., et al., *Fiji: an open-source platform for biological-image analysis*. Nat Methods, 2012. **9**(7): p. 676-82.
76. Li, Y. and J. Andrade, *DEApp: an interactive web interface for differential expression analysis of next generation sequence data*. Source Code for Biology and Medicine, 2017. **12**(1): p. 2.
77. Vlachos, I.S., et al., *DIANA-miRPath v3.0: deciphering microRNA function with experimental support*. Nucleic Acids Research, 2015. **43**(Web Server issue): p. W460-W466.
78. Karagkouni, D., et al., *DIANA-TarBase v8: a decade-long collection of experimentally supported miRNA–gene interactions*. Nucleic Acids Research, 2018. **46**(Database issue): p. D239-D245.
79. Babicki, S., et al., *Heatmapper: web-enabled heat mapping for all*. Nucleic Acids Res, 2016. **44**(W1): p. W147-53.
80. Gawor, M., et al., *Circulating biomarkers of hypertrophy and fibrosis in patients with hypertrophic cardiomyopathy assessed by cardiac magnetic resonance*. Biomarkers, 2018: p. 1-7.

81. Meijers, W.C., A.R. van der Velde, and R.A. de Boer, *ST2 and Galectin-3: Ready for Prime Time?* Ejifcc, 2016. **27**(3): p. 238-52.
82. da Costa Martins, P.A., et al., *MicroRNA regulation in cardiovascular disease*. Curr Drug Targets, 2010. **11**(8): p. 900-6.
83. da Costa Martins, P.A., et al., *MicroRNA-199b targets the nuclear kinase Dyrk1a in an auto-amplification loop promoting calcineurin/NFAT signalling*. Nat Cell Biol, 2010. **12**(12): p. 1220-1227.
84. Castoldi, G., et al., *MiR-133a regulates collagen 1A1: Potential role of miR-133a in myocardial fibrosis in angiotensin II-dependent hypertension*. Journal of Cellular Physiology, 2012. **227**(2): p. 850-856.
85. van Rooij, E., et al., *Dysregulation of microRNAs after myocardial infarction reveals a role of miR-29 in cardiac fibrosis*. Proc Natl Acad Sci U S A, 2008. **105**(35): p. 13027-32.
86. Kriegel, A.J., et al., *The miR-29 family: genomics, cell biology, and relevance to renal and cardiovascular injury*. Physiological Genomics, 2012. **44**(4): p. 237-244.
87. Law, C.W., et al., *voom: precision weights unlock linear model analysis tools for RNA-seq read counts*. Genome Biology, 2014. **15**(2): p. R29.
88. Tao, L., et al., *Exercise Training Protects Against Acute Myocardial Infarction via Improving Myocardial Energy Metabolism and Mitochondrial Biogenesis*. Cell Physiol Biochem, 2015. **37**(1): p. 162-75.
89. Frangogiannis, N.G., *The extracellular matrix in myocardial injury, repair, and remodeling*. The Journal of Clinical Investigation, 2017. **127**(5): p. 1600-1612.
90. Weinberg, E.O., et al., *Expression and regulation of ST2, an interleukin-1 receptor family member, in cardiomyocytes and myocardial infarction*. Circulation, 2002. **106**(23): p. 2961-6.
91. Kakkar, R. and R.T. Lee, *The IL-33/ST2 pathway: therapeutic target and novel biomarker*. Nature reviews. Drug discovery, 2008. **7**(10): p. 827-840.
92. Demyanets, S., et al., *Components of the interleukin-33/ST2 system are differentially expressed and regulated in human cardiac cells and in cells of the cardiac vasculature*. J Mol Cell Cardiol, 2013. **60**: p. 16-26.
93. Chen, W.-Y. and R. Lee, *IL-33/ST2 signaling is anti-cardiac hypertrophic and spatially restricted in cardiomyocytes after pressure overload*. The FASEB Journal, 2015. **29**(1_supplement): p. 942.8.
94. Boyd, W.D., J.V. Tyberg, and J.L. Cox, *A review of the current status of pericardial closure following cardiac surgery*. Expert Rev Cardiovasc Ther, 2012. **10**(9): p. 1109-18.
95. Suryadevara, K., et al., *Evaluation of soluble ST2 as a novel cardiovascular biomarker in patients with acute myocardial infarction*. 2016, 2016. **4**(12): p. 5.
96. Zeyda, M., et al., *Severe obesity increases adipose tissue expression of interleukin-33 and its receptor ST2, both predominantly detectable in endothelial cells of human adipose tissue*. International Journal Of Obesity, 2012. **37**: p. 658.

97. Ho, J.E., et al., *Soluble ST2 predicts elevated SBP in the community*. J Hypertens, 2013. **31**(7): p. 1431-6; discussion 1436.
98. Xia, J., et al., *Increased IL-33 expression in chronic obstructive pulmonary disease*. Am J Physiol Lung Cell Mol Physiol, 2015. **308**(7): p. L619-27.
99. Daniel, M.M.P.J.M.L.B.W.V.P.C.J.C.P.R.P.I.R.P.C.S.U.C.H., *Levels of soluble ST2 in patients with peripheral arterial disease*, in *19. Kardiologie Kongress Innsbruck*. 2017: Innsbruck.
100. Sun, T., et al., *The Role of MicroRNAs in Myocardial Infarction: From Molecular Mechanism to Clinical Application*. International Journal of Molecular Sciences, 2017. **18**(4): p. 745.
101. Yuan, J., et al., *Mir-21 Promotes Cardiac Fibrosis After Myocardial Infarction Via Targeting Smad7*. Cell Physiol Biochem, 2017. **42**(6): p. 2207-2219.
102. Zhou, X.l., et al., *miR-21 promotes cardiac fibroblast-to-myofibroblast transformation and myocardial fibrosis by targeting Jagged1*. Journal of Cellular and Molecular Medicine, 2018. **22**(8): p. 3816-3824.
103. Høfsten, D.E., et al., *Abnormal Glucose Metabolism in Acute Myocardial Infarction*. Influence on Left Ventricular Function and Prognosis, 2009. **2**(5): p. 592-599.
104. Gumbiner, B.M. and N.-G. Kim, *The Hippo-YAP signaling pathway and contact inhibition of growth*. Journal of Cell Science, 2014. **127**(4): p. 709-717.
105. Wang, J., et al., *The Hippo pathway in the heart: pivotal roles in development, disease, and regeneration*. Nature Reviews Cardiology, 2018.
106. Zhou, W. and M. Zhao, *How Hippo Signaling Pathway Modulates Cardiovascular Development and Diseases*. Journal of Immunology Research, 2018. **2018**: p. 8.

CHAPTER VI – ANNEXES

Supplementary Table 1: Spearman correlation statistical values obtained by comparison from ST2 levels measured in both biological fluids and LVEF.

Comparisons	r-value	p-value
PF vs LVEF	-0,098	0,650
PF CTRL vs LVEF	0,707	0,233
PF MI vs LVEF	-0,278	0,249
Plasma vs LVEF	-0,336	0,200
Plasma CTRL vs LVEF	0,707	0,233
Plasma MI vs LVEF	-0,336	0,188

Supplementary Table 2: Spearman correlation statistical values obtained by comparison from relative expression of miR-21-5p, miR-29a-3p and miR-29c-3p with LVEF.

Comparisons	r-value	p-value
miR-21-5p		
miR-21 PF vs LVEF	-0,187	0,429
miR-21 PF CTRL vs LVEF	-	-
miR-21 PF MI vs LVEF	0,075	0,790
miR-21 Plasma vs LVEF	-0,365	0,201
miR-21 Plasma CTRL vs LVEF	-	-
miR-21 Plasma MI vs LVEF	-0,433	0,250
miR-29a-3p		
miR-29a PF vs LVEF	-0,126	0,588
miR-29a PF CTRL vs LVEF	-0,354	0,400
miR-29a PF MI vs LVEF	-0,068	0,799
miR-29a Plasma vs LVEF	-0,148	0,596
miR-29a Plasma CTRL vs LVEF	-	-
miR-29a Plasma MI vs LVEF	-0,033	0,948
miR-29c-3p		
miR-29c PF vs LVEF	-0,098	0,672
miR-29c PF CTRL vs LVEF	-0,359	0,400
miR-29c PF MI vs LVEF	-0,081	0,761
miR-29c Plasma vs LVEF	0,103	0,596
miR-29c Plasma CTRL vs LVEF	-	-
miR-29c Plasma MI vs LVEF	-0,350	0,359